



JOHANNES KEPLER

UNIVERSITÄT LINZ

Netzwerk für Forschung, Lehre und Praxis



Fourier Transform Infrared Spectroscopy of Organic Dielectric / Organic Semiconductor Interface

DIPLOMARBEIT

zur Erlangung des akademischen Grades

DIPLOMINGENIEUR

in der Studienrichtung

TECHNISCHE PHYSIK

Angefertigt am *Linzer Institut für Organische Solarzellen (LIOS)*

Betreuung:

o. Univ.-Prof. Dr. Serdar N. Sariciftci

Eingereicht von:

Pinar Frank

Linz, Oktober 2007

Johannes Kepler Universität

A-4040 Linz · Altenbergerstraße 69 · Internet: <http://www.jku.at> · DVR 0093696

Eidesstattliche Erklärung

Ich erkläre an Eides statt, dass ich die vorliegende Diplomarbeit selbstständig und ohne fremde Hilfe verfasst, andere als die angegebenen Quellen und Hilfsmittel nicht benutzt bzw. die wörtlich oder sinngemäß entnommenen Stellen als solche kenntlich gemacht habe.

Linz, im Oktober 2007

Pinar Frank

*"There are only two ways to live your life. One is as though nothing is a miracle.
The other is as though everything is a miracle."*

A. Einstein

Acknowledgements

First of all I want to thank to my family: my parents, my brother Deniz and my husband Sebastian for supporting me and being there for me whenever I needed them in the past years during my studies of physics.

Further I want to thank Prof. Dr. Serdar Sariciftci for his advice and guidance during this work and for teaching me not only about physics but also about life.

Special thanks to Dr. Birendra Singh who taught me a lot about organic field effect transistors and to Dr. Helmut Neugebauer for introducing me to FTIR-spectroscopy.

For his help during the device fabrication and fruitful discussions I want to thank Gerardo Hernandez Sosa from the Institute of Solid State Physics and all the members of LIOS, especially Robert Koepe, Philipp Stadler and Gebhard Matt for the productive discussions in the coffee kitchen and for the nice time I spent at the institute.

We are very grateful to Polycera (polyimid) and Shin-Etsu (CyEPL) for their supply of dielectric materials used for this work.

Abstract

Research in organic field effect transistors in the last two decades have lead to the major technological advancement as well as to fundamental research towards understanding charge transport, metal-organic semiconductor interface and organic semiconductor-dielectric interface as well as light absorption and emission in the active semiconductor. Among all these phenomena, the interfacial effect of different dielectric materials (insulators) with that of semiconducting material plays a critical role to enable electron (or hole) transport or transport of both types of charge carriers (ambipolar transport). In all the above mentioned phenomena, as a result of an applied field, there is formation of a conducting channel of accumulated charges in the active layer. As a major part of this thesis we have investigated the phenomenon at the semiconductor-insulator-interface by employing the FTIR spectroscopy in transmission mode. FTIR spectroscopy was performed on operating devices, namely, Metal-Insulator-Semiconductor-Metal (MIS) structures as well as organic field-effect transistors (OFETs). Results based on FTIR spectra show strong field-induced absorption for both MIS and transistor geometry. Observation of field-induced absorption indicates formation of a conducting channel due to accumulation of the charge carriers at the interface.

Zusammenfassung

In den letzten 20 Jahren führte die Erforschung der organischen Feld-Effekt Transistoren sowohl zu einem technologischen Durchbruch als auch zu neuen Erkenntnissen in der Grundlagenforschung über den Ladungstransport, die Grenzschicht zwischen Metall und organischem Halbleiter, die Grenzschicht zwischen Isolator und organischem Halbleiter und über die Absorption und Emission von Licht im aktiven Halbleiter. Unter all diesen Phänomenen spielt der Grenzschichteffekt verschiedener dielektrischer Materialien (Isolatoren) mit halbleitenden Materialien eine besondere Rolle bei der Ermöglichung des Elektron- (oder Loch-) Transports, oder des Transports der beiden Ladungsträger (ambipolarer Transport). In allen eingangs erwähnten Phänomenen bildet sich nach Anlegen eines Feldes ein leitender Kanal aus, bestehend aus angesammelten Ladungen in der aktiven Schicht. Ein Grossteil dieser Arbeit beschäftigt sich mit der Erforschung des Phänomens an der Halbleiter-Isolator-Grenzfläche mittels der Anwendung der FTIR-Spektroskopie im Transmissionsmodus. Zur Untersuchung mittels FTIR-Spektroskopie wurden sowohl Metall-Isolator-Halbleiter-Metallstrukturen (MIS) als auch organische Feld-Effekt Transistoren (OFETs) verwendet. Es zeigt sich anhand der FTIR-Spektren eine starke feldinduzierte Absorption sowohl für MIS als auch für Transistoren. Die Beobachtung dieser feldinduzierten Absorption weist auf die Bildung eines leitenden Kanals aufgrund der Ansammlung der Ladungsträger an der Grenzfläche hin.

Table of Contents

| | |
|---|----|
| 1. Introduction | 1 |
| 1.1. Organic Transistors | 1 |
| 1.1.1. Simplified Working Principles of FETs:..... | 3 |
| 1.1.2. Basic Operating Regimes of a Field-Effect Transistor | 3 |
| 1.1.3. Operating Principle of OFETs: | 5 |
| 1.1.4. Characterisation of FETs..... | 6 |
| 1.1.5. Gate Dielectrics for Organic Field-Effect Transistors: | 7 |
| 1.1.6. Organic semiconductors for Organic Field-Effect Transistors | 9 |
| 1.2. Infrared Spectroscopy | 13 |
| 1.2.1 Michelson Interferometer | 13 |
| 1.2.2 Fourier Transformed Infrared Spectroscopy | 14 |
| 1.2.3 Fourier Transform | 15 |
| 1.2.4. ATR method | 17 |
| 2. Experimental | 19 |
| 2.1. Role of organic dielectrics on the charge transport properties in OFETs..... | 19 |
| 2.1.1 Devices with Pentacene..... | 22 |
| 2.2.2 Devices with Zinc Phthalocyanine..... | 22 |
| 2.2. Device fabrication and characterisation for FTIR measurements..... | 22 |
| 2.3. FTIR measurements | 25 |
| 2.4. List of Instruments | 28 |
| 2.5. List of Materials | 29 |
| 3. Results and Discussion..... | 30 |
| References | 46 |
| List of Figures | 52 |
| Curriculum Vitae..... | 56 |

1. Introduction

My thesis is organised as follows: first I present a brief introduction to organic field effect transistor, its working principles and relevant materials as well as working principles of FTIR spectroscopy are also briefly introduced. In the second part of my thesis I present the experimental procedures and devices employed to investigate interfacial effects of OFETs. In the third part, results and discussion are presented.

1.1. Organic Transistors

An organic field effect transistor (OFET) requires the following components:

a thin *semiconducting layer*, which is separated from a *gate electrode* by the *insulating dielectric* and a *source* and a *drain* electrode in contact with the semiconducting layer.

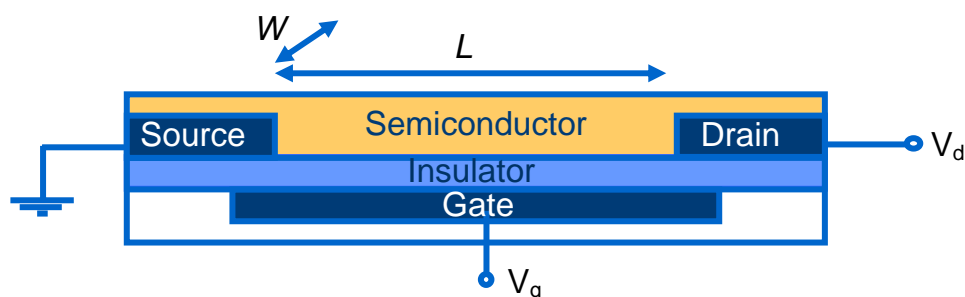


Figure 1 Schematic structure of a bottom gate bottom contact OFET

In OFETs, which have been investigated since 1986 when the first device was demonstrated using non-substituted polythiophenes [1], the semiconducting thin layer is usually vacuum sublimed, spin-coated or drop-cast depending on its physical properties. The gate electrode can be a metal but very often highly doped silicon serves as substrate and gate electrode at once. As gate dielectric there are three different classes: high dielectric constant (ϵ) inorganic insulators such as e.g. SiO_2 , Al_2O_3 , SiN_x , polymeric insulators such as e.g. poly(methylmethacrylate) (PMMA) or polyvinylphenol (PVP), and self assembled monolayers (SAMs), used depending on the transistor structure and desired properties [2]. The source and the drain electrodes, which inject charges into the semi conductor are usually metals such as gold but conducting polymers (e.g. PEDOT:PSS) which can be inkjet printed are also used. The organic field-effect transistors have been developed to realize low-cost, large-area electronic devices [3].

The source electrode is normally grounded ($V_s = 0$), gate voltage (V_g) and drain voltage (V_d) are applied to the gate and drain electrodes respectively. The source electrode injects charges as it is more negative than the gate electrode when a positive gate voltage is applied (electrons are injected) and more positive than the gate electrode when a negative gate voltage is applied (holes are injected). [4]

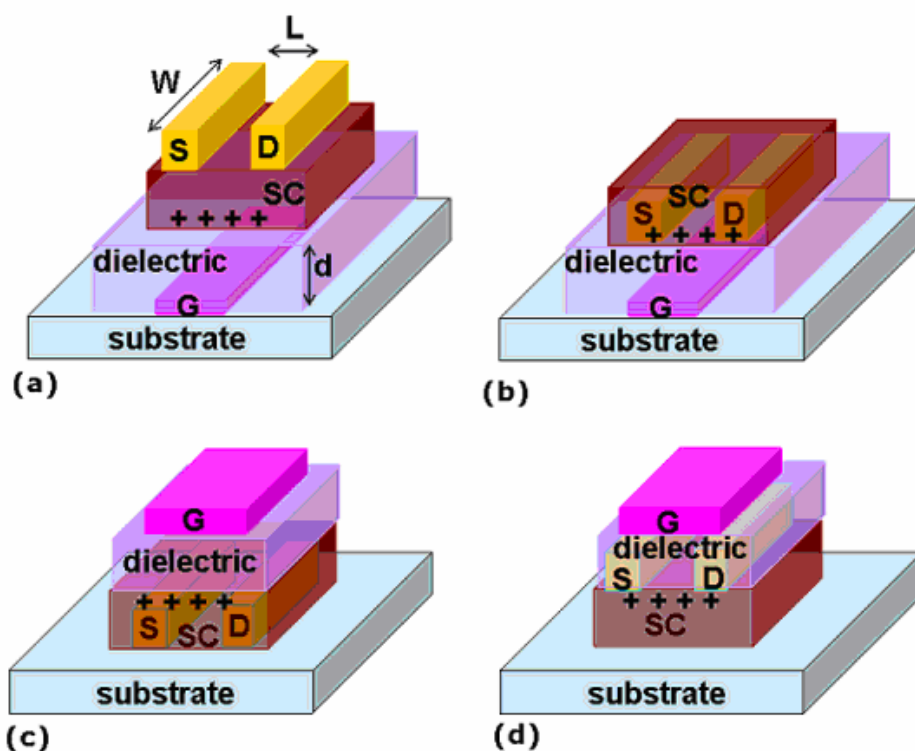


Figure 2 Possible device structures commonly used for organic field effect transistors. a) top contact / bottom gate, b) bottom contact / bottom gate, c) bottom contact / top gate, d) top contact / top gate [3]

OFETs have been fabricated with various device geometries as shown in Figure 2. The most commonly used geometry is a bottom gate with top contact, partly because it borrows the concept of silicon TFT, using thermally grown Si/SiO₂ as dielectric. Because it is commercially available high quality Si/SiO₂ substrate, this device geometry has dominated the field. Recently it was shown that organic dielectrics are also promising for high performance OFETs. Organic dielectrics have the following advantages compared to the Si/SiO₂ substrate: (1) they can be solution processed, (2) provide smooth films on transparent glass and plastic substrates, (3) are suitable for optoelectronics like photoresponsive OFETs because of their high optical transparency, (4) can be thermally stable up to 200°C with relatively small thermal-expansion coefficient, and (5) can possess a rather high dielectric constant up to 18. [3]

1.1.1. Simplified Working Principles of FETs:

Without applying any voltage to the gate electrode ($V_g = 0$) the organic semiconductor, which is intrinsically undoped, will not show any charge carriers. The only way to create flowing current in the semiconductor is direct injection from the source/drain electrodes (Figure 3 a)

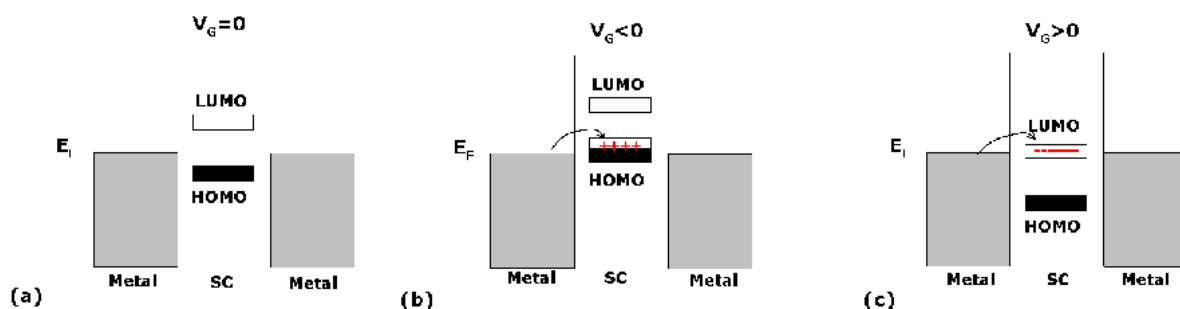


Figure 3 Energy level diagrams explaining the working principles of an OFET [3]

When a negative voltage is applied to the gate electrode ($V_g < 0$), positive charges are induced at the organic semiconductor – dielectric interface (a p-type conducting channel is formed) (Figure 3 b). If the Fermi level of the source/drain metal is close to the HOMO level of the organic semiconductor, positive charges can be extracted by the electrodes by applying a voltage, V_d , between the source and drain.

When a positive gate voltage is applied ($V_g > 0$), negative charges are induced at the organic semiconductor – dielectric interface (an n-type conducting channel is formed) (Figure 3 c). If the Fermi level of the source/drain metal is close to the LUMO level of the organic semiconductor, then negative charges can be extracted by the electrodes by applying a voltage, V_d , between the source and drain.

Organic semiconductors with the ability to conduct only positive (negative) charge carriers are called p-type (n-type) semiconductors. In some organic semiconductors, both electrons and holes can be injected and transported which allows the fabrication of ambipolar transistors.

1.1.2. Basic Operating Regimes of a Field-Effect Transistor

As shown in Figure 4 below there are three basic operating regimes for OFETs. For the case that the gate potential exceeds the threshold voltage V_{Th} , which describes an activation potential for channel formation ($V_g > V_{th}$): when a low drain voltage is applied ($V_d \ll V_g - V_{th}$), the current flowing through the channel is directly proportional to

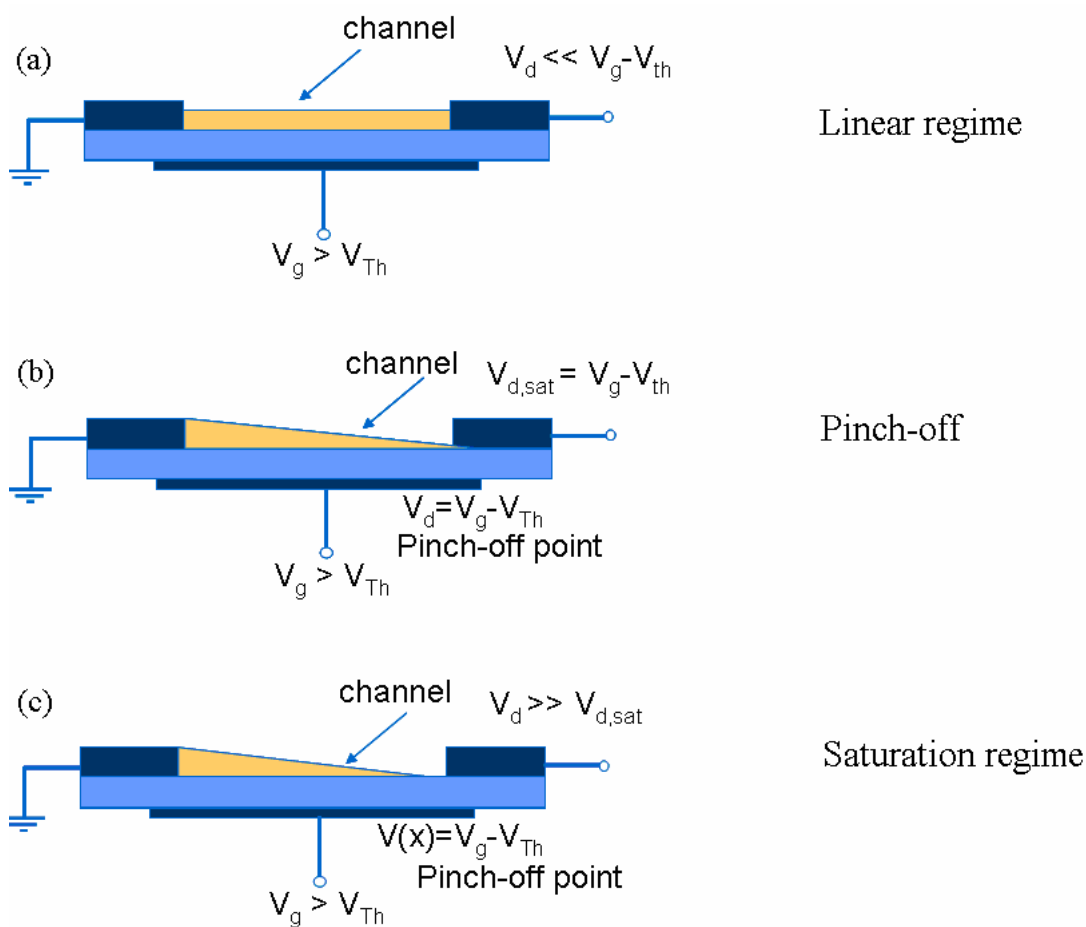


Figure 4 Cross section of an OFET in three basic operation regimes: (a) for $V_d \ll V_g - V_{th}$ I_{ds} is linearly depending on V_d (linear regime), (b) At $V_d = V_g - V_{th}$ the conductive channel is pinched off, (c) for $V_d \gg V_d$ I_{ds} doesn't depend on V_d and has a constant value (saturation regime) [5]

V_d . (Figure 4 a). When the source-drain voltage is further increased, a point is reached where $V_d = V_g - V_{th}$ at which the channel is “pinched off” (Figure 4 b). That means a depletion region is formed next to the drain because the difference between the local potential V and the gate voltage is now below the threshold voltage. A space charge limited saturation current $I_{d,sat}$ can flow across this narrow depletion zone as carriers are swept from the pinch-off point to the drain by the comparatively high electric field in the depletion mode. Further increasing the source drain voltage will not increase the current but leads to an expansion of the depletion region. Since the potential at the pinch-off point remains $V_g - V_{th}$ and thus the potential drop between that point and the source electrode stays the same the current saturates at a level $I_{d,sat}$ (Figure 4 c); this regime is called the saturation regime. [5]

1.1.3. Operating Principle of OFETs:

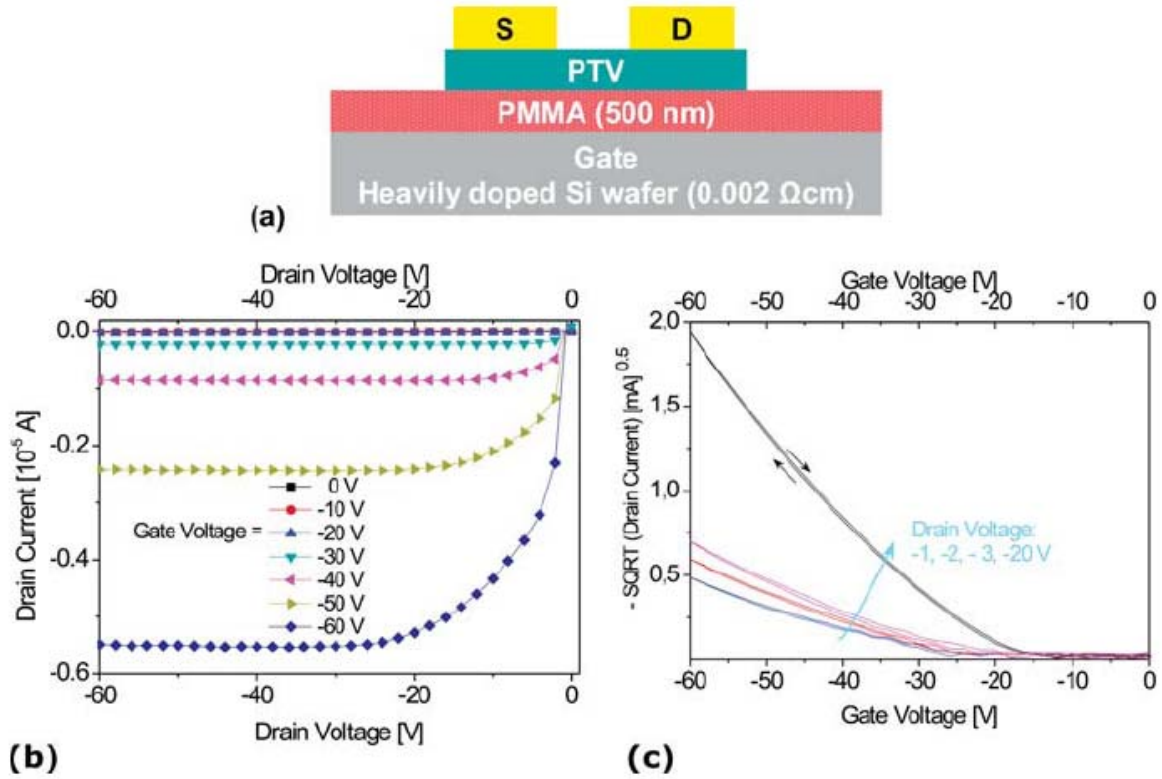


Figure 5 (a) Scheme of top contact PTV OFET. (b) Output characteristics (I_{ds} versus V_d) of a p-channel PTV OFET. (c) Transfer characteristics ($\sqrt{I_{ds}}$ versus V_g for different V_d). Linear field effect mobility of $7 \times 10^{-4} \text{ cm}^2 \text{Vs}^{-1}$ and saturated mobility of $10^{-3} \text{ cm}^2 \text{Vs}^{-1}$ can be extracted from these devices with channel length L of $25 \mu\text{m}$ and channel width W of 1.4 mm ($W/L = 40$). [3]

A poly(2,3-thienylene vinylene) (PTV) OFET with PMMA as gate insulator on top of highly doped Si substrate as gate electrode is used here to describe typical OFET device characteristics and the methods for calculating the mobility μ and the I_{on}/I_{off} ratio. The OFET I-V characteristics can be adequately described by standard models. [4][37][38][39]

At low V_d , I_{ds} increases linearly with V_d (linear regime) and is approximately given by the following equation:

$$I_{d,linear} = \frac{W}{L} \mu_{linear} C_i (V_g - V_{th}) V_d \dots \text{linear regime} \quad (1)$$

W ...channel width, C_i ...capacitance, V_g ...gate voltage,
 L ...channel length, I_d ...drain current, V_{th} ...threshold voltage

The field effect mobility can be calculated in the linear regime from the transconductance g_m ,

$$|g_m|_{\text{linear}} = \left(\frac{\delta I_{ds}}{\delta V_g} \right)_{V_{ds}=\text{const}} = \frac{W}{L} \int_0^{V_{ds}} \mu C_i dV = \frac{WC_i}{L} \mu V_{ds} \quad (2)$$

by plotting I_{ds} versus V_g at low V_d and equating the value of the slope of this plot to g_m .

When V_d is more negative than V_g , I_{ds} tends to saturate (saturation regime) owing the pinch-off of the accumulation layer, and this regime is determined from the following equation:

$$I_{d,\text{saturated}} = \frac{W}{2L} \mu_{\text{saturated}} C_i (V_g - V_{th})^2 \dots \text{saturation regime} \quad (3)$$

In the saturation regime, μ can be calculated from the slope of the plot of $\sqrt{I_{ds}}$ versus V_g , as shown in Figure 5 c

$$\mu = \frac{d\sqrt{I_d}}{dV_g} \frac{2L}{WC_i} \dots \text{calculation of the mobility} \quad (4)$$

The difference between calculated μ values is assigned to higher charge-carrier density in the saturation regime as compared with that of the linear regime. [3]

1.1.4. Characterisation of FETs

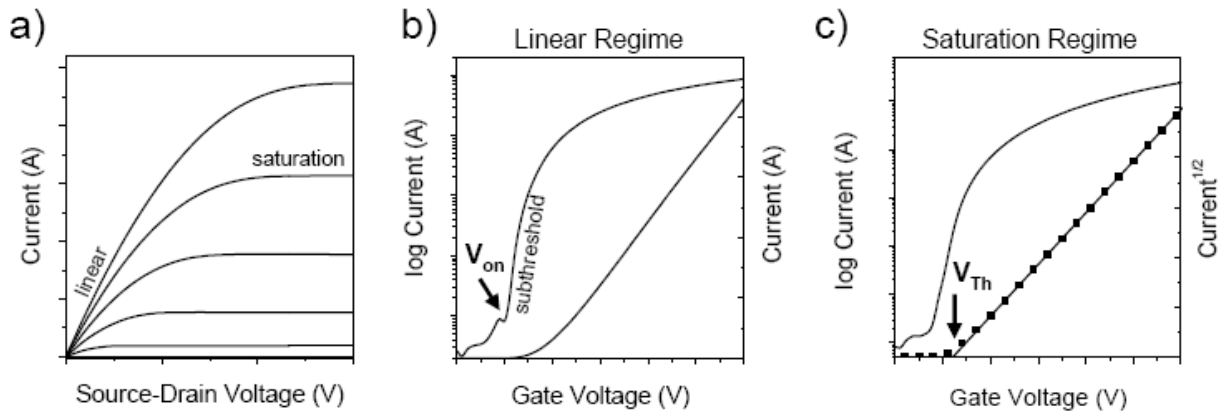


Figure 6 Representative current-voltage curves of an n-channel organic field effect transistor. (a) Output characteristics indicating linear and saturation regime. (b) Transfer characteristics in the linear regime indicating the onset voltage (V_{on}) where the drain current increases abruptly. (c) Transfer characteristics in the saturation regime indicating the threshold voltage V_{th} where the linear fit to the square root of the drain current intersects with the x axis.

Organic field effect transistors are characterised by output and transfer curves. Typical output characteristics which is the drain current I_d plotted versus source-drain voltage V_d for different

constant gate voltages ($V_g = const$) are shown in Figure 6 a for an n-channel transistor. From the output characteristics the linear regime at low V_d and the saturation regime at high V_d are evident.

In transfer characteristics the drain current I_d is plotted versus gate voltage V_g at a constant drain Voltage V_d . Figure 6 b shows the transfer characteristics of the same n-channel transistor in the linear regime ($V_d \ll V_g$) both as semi log and linear plot. From the semi log plot one can easily extract the onset voltage V_{on} at which the drain current abruptly increases above a defined low off-current level. Ideally the onset voltage and the threshold voltage should be the same or very similar. The gradient of the current increase in the linear regime is directly proportional to the mobility according to equation (1). Figure 6 c shows a transfer curve in the saturation regime. Here the square root of the drain current should be linearly dependent on the gate voltage and its gradient is proportional to the mobility according to equation (4). Extrapolating the linear fit to zero gives the threshold voltage V_{th} .

A high threshold voltage indicates a large number of traps at the dielectric/semiconductor interface. This leads to a threshold shift during the measurements evident as hysteresis, which is the difference between the forward and reverse scan, of the current-voltage characteristics. [5]

Furthermore, if there is a condition arises with an applied V_d and V_g where not only source electrode injects charges but also drain electrode injects different polarity of charge carriers forming a conducting channel of two types of carriers in the semiconducting layer leads to ambipolar OFET. Ambipolar OFETs are well suited for various fundamental studies and applied to device applications such as light emitting transistors, inverter circuits, and provide a simple device to compare μ of different charge carrier under the identical conditions. However, ambipolar OFETs are very critical to the choice of the gate dielectrics and contact electrode as well as environmental conditions. [5]

1.1.5. Gate Dielectrics for Organic Field-Effect Transistors:

Considering the various OFET structures and the implications of Equations (1) and (3), it becomes immediately evident that for the manufacture of high-quality OFETs, the organic semiconductor is not the only critical component. It is also very important to incorporate a suitable gate insulator. The critical parameters are the maximum possible electric displacement D_{max} the gate insulator can sustain,

$$D_{\max} = \epsilon_0 \epsilon E_B \quad (8)$$

Where epsilon is the dielectric constant, E_B is the dielectric breakdown field; and the capacitance per area C_i is

$$C_i = \epsilon_0 (\epsilon / d) \quad (9)$$

with d as the insulator thickness. The capacitance magnitude is governed not only by the ϵ value but also by the thickness d for which a pinhole-free film can be achieved, and thus may reflect the deposition procedure as well as intrinsic materials properties.

Solution processable gate dielectrics are very attractive for applications in electronics, in part because films exhibiting good characteristics can often be formed simply by spin coating, casting or printing at room temperature and under ambient conditions. Moreover the characteristics of polymers can be tuned by the design of the monomer precursor and polymerisation reaction conditions. The result is that polymers exhibiting a broad and complementary solubility and processability and dielectric properties (ϵ values) can be selected for application in many electronic devices (Figure 12). The first detailed study investigating the effect of different polymeric insulators on organic semiconductor field-effect mobilities was reported by Peng et al. [7]. By investigating transistors with various insulators (CyEPL, PVA, PVC, PMMA, PS) Peng et al [7] reported a strong correlation between the insulator ϵ values and the field-effect mobility. In 2002, Klauk et al. reported in detail on the properties of PVP-based dielectrics, comparing cross linked PVP with PVP copolymer and reporting that the cross linked PVP exhibits greater insulating properties than the PVP copolymer [8]. In a recent paper, Veres et al. reported [9] that the interaction between the insulator and semiconductor materials plays an important role in carrier transport, but not only by influencing the morphology of the overlying semiconductor. Very recently, [10] Chua et al. showed that the use of hydroxyl-free gate dielectric such as BCB can yield n-channel FET conduction in most conjugated polymers. In fact, one characteristic feature of most polymeric semiconductors is the strong trapping of electrons but not holes, with FETs typically exhibiting p-type, but not n-type, conduction. Even with the appropriate low-work-function electrodes. The authors' results show that in FETs, electrons are considerably more mobile in typical semiconducting materials than generally thought. The authors further elaborate that the reason why n-type behaviour has previously been so elusive is the trapping (destructive reaction) of electrons at the semiconductor/dielectric interface by hydroxyl functionalities, present in form of silanol groups in the case of the commonly used SiO_2 dielectric films [10][2]. Nevertheless these findings are not completely true because dielectrics such as PVA

with hydroxyl functionalities also enable electron transport [5] and these results have also been a motivation for the systematic study of organic dielectric and organic semiconductor interface in terms of ambipolar transport.

1.1.6. Organic semiconductors for Organic Field-Effect Transistors

In this section the evolution of organic semiconductors for use in OFETs is presented with respect to their processing conditions and field-effect μ in Table 1. The chemical structures of most commonly used p-type and n-type semiconductors are presented in Figure 7 and 8.

Table 1 Highest field-effect mobility (μ) values measured from OTFTs as reported in the literature annually from 1986 through 2005. (taken from [3])

| <i>Year</i> | <i>Mobility (cm²/Vs)</i> | <i>Material (deposition method)*</i> | <i>I_{on}/I_{off}**</i> | <i>W/L</i> | <i>Reference</i> |
|-------------|-------------------------------------|--|---|------------|------------------|
| 1983 | Minimal, not reported (NR) | Polyacetylene (s) (demonstration of field effect in an OTFT) | NR | 200 | [43] |
| 1986 | 10 ⁻⁵ | Polythiophene (s) | 10 ³ | NR | [1] |
| 1988 | 10 ⁻⁴ | Polyacetylene (s) | 10 ⁵ | 750 | [44] |
| | 10 ⁻³ | Phthalocyanine (v) | NR | 3 | [45] |
| | 10 ⁻⁴ | Poly(3-hexylthiophene) (s) | NR | NR | [46] |
| 1989 | 10 ⁻³ | Poly(3-alkylthiophene) (s) | NR | NR | [47] |
| | 10 ⁻³ | α - ω -hexathiophene (v) | NR | NR | [48] |
| 1992 | 0.027 | α - ω -hexathiophene (v) | NR | 100 | [49] |
| | 2 x 10 ⁻³ | Pentacene (v) | NR | NR | [49] |
| 1993 | 0.05 | α - ω -di-hexyl-hexathiophene (v) | NR | 100–200 | [50] |
| 1994 | 0.06 | α - ω -dihexyl-hexathiophene (v) | NR | 50 | [51] |
| 1995 | 0.03 | α - ω -hexathiophene (v) . | >10 ⁶ | 21 | [52] |
| | 0.038 | Pentacene (v) | 140 | 1000 | [53] |
| | 0.3 | C ₆₀ (v) | NR | 25 | [54] |
| 1996 | 0.02 | Phthalocyanine (v) | 2x 10 ⁵ | NR | [20] |
| | 0.045 | Poly(3-hexylthiophene) (s) | 340 | 20.8 | [55] |
| | 0.13 | α - ω -dihexyl-hexathiophene (v) . | >10 ⁴ | 7.3 | [56] |
| | 0.62 | Pentacene (v) | 10 ³ | 11 | [57] |

| Year | Mobility (cm ² /Vs) | Material (deposition method)* | I_{on}/I_{off} ** | W/L | Reference |
|------|--------------------------------|---|-----------------------|------|-----------|
| 1997 | 1.5 | Pentacene (v) | 10 ⁸ | 2.5 | [58] |
| | 0.05 | Bis(dithienothiophene) (v) | 10 ⁸ | 500 | [59] |
| 1998 | 0.1 | Poly(3-hexylthiophene) (s) | >10 ⁶ | 20 | [32] |
| | 0.23 | α - ω -dihexyl-quaterthiophene (v) | NR | 1.5 | [60] |
| | 0.15 | Dihexyl-anthradithiophene | NR | 1.5 | [61] |
| 2000 | 0.1 | n-decapentafluoroheptyl -methylnaphthalene- 1,4,5,8-tetracarboxylic diimide (v) | 10 ⁵ | 1.5 | [62] |
| | 0.1 | α - ω -dihexyl-quinquethiophene (s) | NR | NR | [62] |
| 2002 | 3 | Pentacene (v) | 10 ⁵ | 1.3 | [63] |
| | 0.6 | N, N'-dioctyl-3,4,9,10-perylene tetracarboxylic diimide (v) | 10 ⁵ | 10 | [64] |
| 2003 | 0.001 | CuPc (v) | 2.3 x 10 ⁴ | 165 | [23] |
| | 0.002 | Methanofullerene [6,6]-phenyl-C ₆₁ - butyric acid methyl ester (s) | NR | 140 | [65] |
| | 0.53 | C ₆₀ (v) | 10 ⁸ | 40 | [66] |
| | 3.3 | Pentacene(v) | 1.6x10 ⁶ | 10 | [67] |
| | 6 | Pentacene(v) | | | [15] |
| | 0.18 | 3', 4'-dibutyl-5,5-bis(dicya nomethylene)-5,5'-dihydro -2,2':5',2''-terthiophene (DCMT) | 10 ⁶ | 10 | [69] |
| 2004 | 0.73 | Poly(3-hexylthiophene) (s) | NR | 12 | [70] |
| | 0.1 | PTCDI-C ₅ (v) | 10 ⁵ | 10 | [71] |
| | 0.004 | C ₆₀ (v) | 10 ⁵ | 250 | [72] |
| | 0.2 | Methanofullerene [6,6]-phenyl-C ₆₁ - butyric acid methyl ester (s) | 10 ³ | 23 | [16] |
| | 0.1 | P3HT (s) | 10 ⁵ | 200 | [73] |
| | 0.01 | Methanofullerene [6,6]-phenyl-C ₆₁ - butyric acid methyl ester (s) | 10 ⁶ | 25 | [74] |
| 2005 | 0.63 | C ₆₀ (v) | 10 ⁴ | 40 | [75] |
| | 0.015 | Poly(3,3''-dialkyl-terthiophene) | 10 ⁵ | 50 | [76] |
| | 6 | C ₆₀ (v) | 10 ⁴ | 40 | [68] |
| | 0.51 | Pentacene (v) | 10 ⁵ | 40 | [77] |
| | 0.06 | C ₆₀ -fused N-methylpyrrolidine- meta-C12 phenyl (C60MC12) (s) | 1.6x 10 ⁵ | 250 | [78] |
| | 0.02 | Methanofullerene [6,6]-phenyl-C ₆₁ - butyric acid methyl ester (s) | 7x 10 ⁴ | 250 | [78] |
| 0.15 | Thieno[2,3-b]thiophene | 10 ⁵ | NR | [79] | |

* (v)...vacuum deposition and (s)...from solution

**Values for I_{on}/I_{off} correspond to different gate voltage ranges and thus are not readily comparable to one another. The reader is encouraged to read the details of the experiments in the cited references.

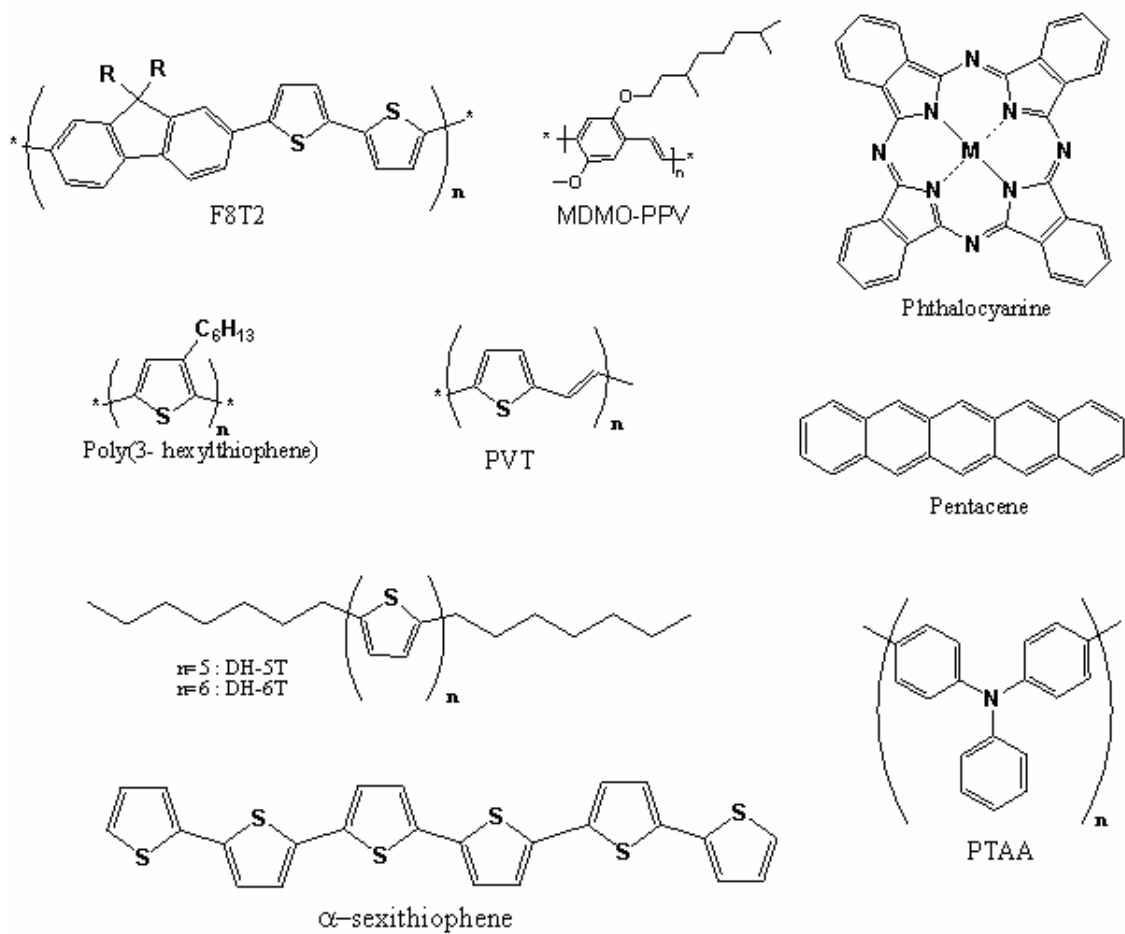


Figure 7 Commonly used p-type organic semiconductor: F8T2 (poly[9,9' dioctyl-fluorene-co-bithiophene]); MDMO-PPV(poly[2-methoxy-5-(3,7-dimethyloctyloxy)-1,4-phenylenevinylene]); P3HT: regioregular poly [3-hexylthiophene]; PTAA: polytriarylamine; PVT: poly-[2,5-thienylene vinylene];, DH-5T: (α, ω-dihexylquinquethiophene); DH-6T: (α, ω-dihexylsexithiophene); phthalocyanine, pentacene, (α-6T) α-sexithiophene.

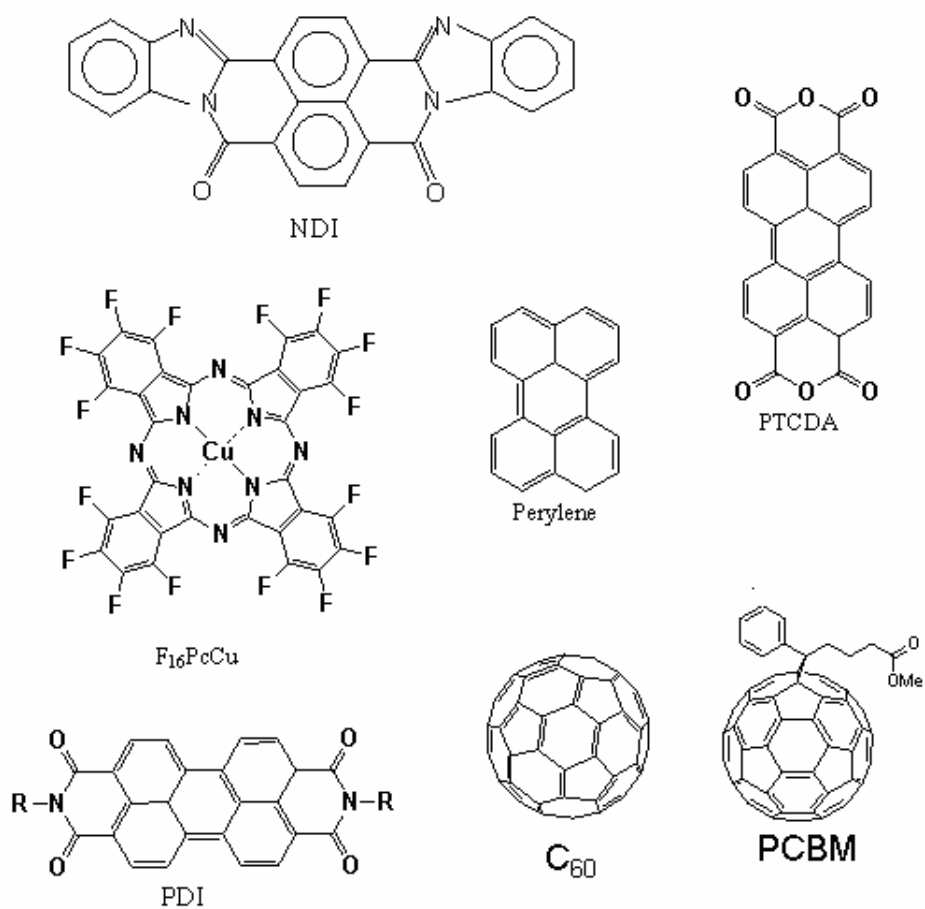


Figure 8 Commonly used n-type organic semiconductor: NDI: naphthalene diimide; F₁₆CuPc :perfluorocopperphthalocyanine; Perylene; PTCDA: 3,4,9,10-perylene-tetracarboxylic dianhydride and its derivatives; PDI: N,N'-dimethyl 3,4,9,10-perylene tetracarboxylic diimide; C₆₀ ; and PCBM : methanofullerene [6,6]-phenyl C₆₁-butyric acid methyl ester.

1.2. Infrared Spectroscopy

1.2.1 Michelson Interferometer

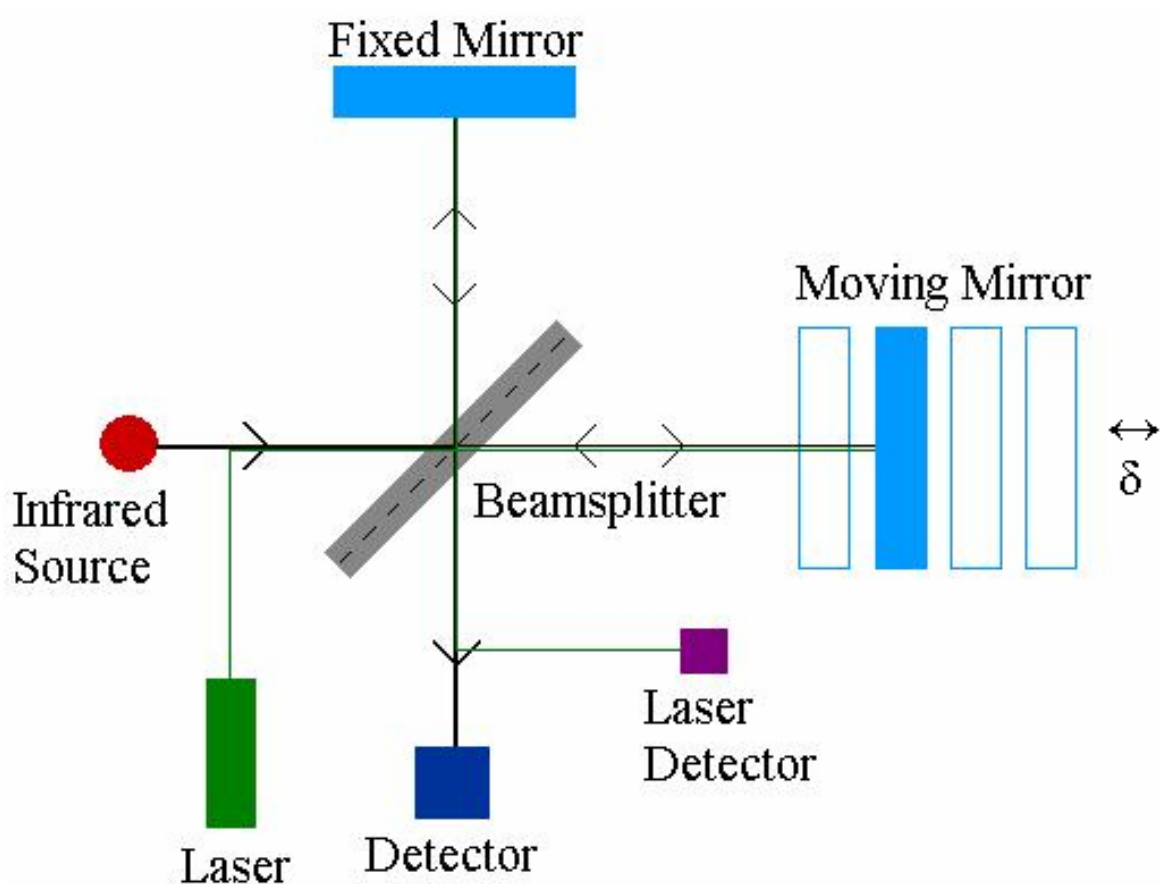


Figure 9 Schematic of a Michelson Interferometer

The heart of an FTIR-spectrometer is the Michelson interferometer. In the simplified Michelson Interferometer, light originates from a broadband infrared source whose output is collimated; this light beam then impinges upon a beamsplitter. The beamsplitter transmits 50% of the light to one mirror, and reflects 50% of the light to a second mirror. The light reflected off these two mirrors is passed / reflected by the beamsplitter a second time, and the two beams recombine on the other side of the beamsplitter, (possibly pass through a sample), and are finally focused onto an infrared detector. In the interferometer, one mirror is held in a fixed position relative to the beamsplitter during the measurement. A second mirror (the moving mirror) scans back and forth relative to the beamsplitter in a continuous fashion. (Figure 9)

1.2.2 Fourier Transformed Infrared Spectroscopy

In a rapid scan FTIR then, the moving mirror in the interferometer does just that: it scans forward and backward in a rapid continuous fashion. During the mirror scan, the path length of the infrared beam from the beamsplitter to the moving mirror changes relative to the path length of the IR beam to the fixed mirror. This path traversal difference for the light beams in the two arms of the interferometer is known as either *the optical path difference* (OPD) or *optical retardation* δ . When the two parts of the infrared beam recombine on the other side of the beamsplitter and form an image at the detector, the intensity of the composite beam is in fact an interference pattern, i.e. the generated intensity depends very strongly upon the optical path difference. The plot of this intensity variation as a function of optical retardation, i.e. the intensity registered at the detector as a function of moving mirror position, is known as *the interferogram* $I(\delta)$. During such a mirror scan the broadband IR light characteristically generates an interferogram as exemplified by Figure 8; the intensity is normally large at the zero path difference (ZPD) position when the two mirrors are equidistant from the beamsplitter, and easy to understand since all wavelengths of light will interfere constructively at the point of zero path difference, whereas in the wings of the interferogram some wavelength will be interfering constructively while others will be interfering destructively.

In the Figure 9, we see that in addition to the infrared beam a Helium-Neon (HeNe) laser beam traverses the same optical path as the infrared light. The monochromatic HeNe beam is split by the beamsplitter and the two beams are also recombined after passing through the two arms of the interferometer, just as for the infrared beam. Because the HeNe laser light is monochromatic, however, it generates a sine-squared interferogram pattern when modulated by the interferometer. That is to say, in an ideal interferometer where the moving mirror moves at a constant velocity, one will observe a constant frequency and constant amplitude interferogram for a monochromatic source such as a laser. The HeNe interferogram is displayed in the lower trace of Figure 10. This HeNe laser interferogram is used by the FTIR to monitor the mirror position during the course of the scan. (Rather than mirror position it is technically more appropriate to refer to the difference in path length that the two beams traverse in going “out and back” from the beamsplitter to each of the two mirrors, hence we speak of the optical path difference.) In this fashion the HeNe laser generates fringes as the mirror moves, and the HeNe light detector electronics “counts” these fringes to determine the

mirror position. As shown in the Figure 10, every time one of these HeNe fringes is generated, the spectrometer electronics are triggered to simultaneously digitize the infrared light intensity registered at the infrared detector. Although in rapid-scan mode the mirror moves in a continuous fashion, we now recognize that the stored IR interferogram is actually a digital point-by-point plot of detector by the HeNe fringes: every time a $\frac{1}{2}$ -HeNe wavelength is completed, the electronics are triggered to read the IR detector output and store the value. As a result of this process one obtains the digital interferogram, i.e. the digital plot of intensity versus mirror position. [12][13]

1.2.3 Fourier Transform

Usually the scientists are interested in transmission or absorption type experiments, where the total light intensity I transmitted after the light passes through a sample is measured as a function of wavelength and ratioed versus the light intensity I_0 recorded when no sample is present. What the Michelson interferometer produces, however, is the interferogram: a digital plot of light intensity versus mirror position (in cm). Only when a mathematical function known as the digital Fourier transform (FT) is applied to the data does one obtain a single beam spectrum of intensity I versus wavenumber (in cm^{-1}).

For a transmission measurement there are actually two experiments that are carried out sequentially: First an interferogram measurement is made with no sample present; this is Fourier-transformed to yield the single beam reference (SBR) or I_0 spectrum. In the next measurement, the sample is placed in the beam, and the mirror is scanned to produce a second interferogram with a different pattern, usually of smaller amplitude due to some of the light being absorbed or scattered by the sample. This second spectrum is then Fourier-transformed to yield the single beam sample (SBS) or I spectrum. Having obtained these two spectra, they can be manipulated in the usual ways to yield either a transmittance $[I / I_0]$ or absorbance $[-\log (I / I_0)]$ spectrum. (Figure 10) [12][13]

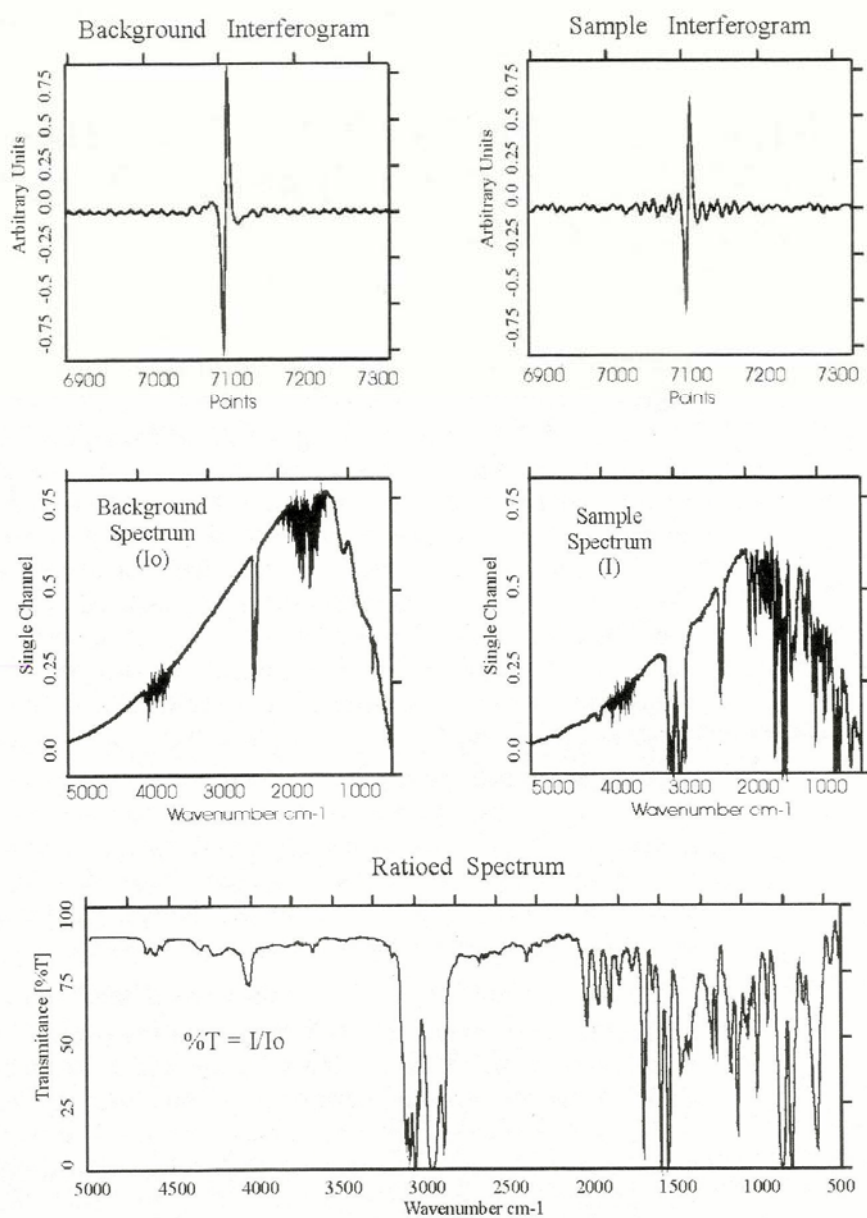


Figure 10 Data collection in FTIR spectroscopy. Two interferograms are recorded. Each of these is Fourier transformed to produce single beam spectra I_0 and I respectively. Finally, I is divided by I_0 to yield the (%T) transmittance spectrum.[12]

1.2.4. ATR method

Attenuated total reflection infrared (ATR-IR) spectroscopy is used for analysis of the surface of materials. It is also suitable for characterization of materials which are either too thick or too strongly absorbing to be analyzed by transmission spectroscopy. For the bulk material or thick film, no sample preparation is required for ATR analysis.

For the attenuated total reflection infrared (ATR-IR) spectroscopy, the infrared radiation is passed through an infrared transmitting crystal with a high refractive index, allowing the radiation to reflect within the ATR element several times.

The sampling surface is pressed into intimate optical contact with the top surface of the crystal such as ZnSe or Ge. The IR radiation from the spectrometer enters the crystal. It then reflects through the crystal and penetrating “into” the sample a finite amount with each reflection along the top surface via the so-called “evanescent” wave. At the output end of the crystal, the beam is directed out of the crystal and back into the normal beam path of the spectrometer.

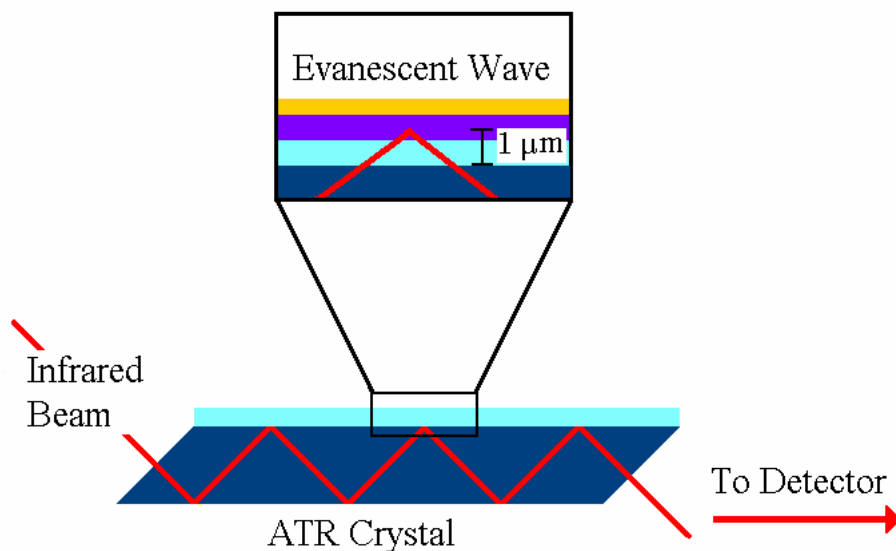


Figure 11 Evanescent wave penetrating in the device (MIS or transistor) built on ATR crystal

To obtain internal reflectance, the angle of incidence must exceed the critical angle θ_c . This angle is a function of the real parts of the refractive indices of both the sample and the ATR crystal:

$$\theta_c = \sin^{-1}(n_1/n_2) \quad (5)$$

Where n_2 is the refractive index of the sample and n_1 is the refractive index of the crystal.

The evanescent wave decays into the sample exponentially with distance from the surface of the crystal over a distance on the order of microns.

$$E = E_0 e^{-z/d_p} \quad (6)$$

The depth of penetration of the evanescent wave d is defined as the distance from the crystal-sample interface where the intensity of the evanescent decays to $1/e$ ($\approx 37\%$) of its original value. It can be given by:

$$d_p = \frac{\lambda_1}{2\pi\sqrt{\sin^2 \theta - n_{21}^2}} \quad (7)$$

where λ is the wavelength of the infrared radiation. [14]

2. Experimental

2.1. Role of organic dielectrics on the charge transport properties in OFETs

For the systematic study of organic dielectrics, numerous devices were fabricated using pentacene and zinc phthalocyanine (chemical structures shown in Figure 13) as semiconductor and various organic dielectrics such as PMMA (polymethyl methacrylate), PVP (polyvinyl phenol), CyEPL (cyanoethylpullulan), PVA (polyvinyl alcohol), BCB (divinyltetra-methyldisiloxanebis(benzocyclobutene)), polyimide (chemical structures shown in Figure 14, dielectric constants are listed in Table 1) The devices were all built with top contact / bottom gate structure on top of glass substrates as shown in Figure 12 below.

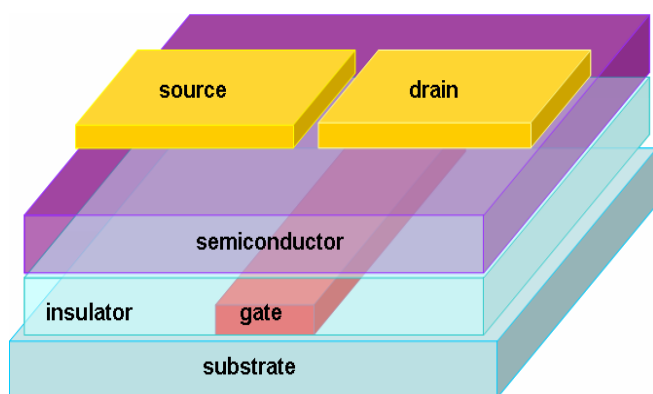


Figure 12 device structure of Bottom Gate / Top Contact organic transistor, used for the systematic study with different organic dielectrics

ITO (indium tin oxide) coated glass substrates (15 mm x 15 mm) were etched to leave an area of 0.5 mm x 15 mm serving as a gate electrode and cleaned with 2% Hellmanex solution in the ultrasonic bath which was followed by further ultrasonic bath with H₂O and then in isopropanol. On top of ITO/glass organic dielectric is applied with spin-coating and baked in the vacuum oven under Ar atmosphere, if necessary, depending on the type of the dielectric as mentioned separately. Standard programme is used for the spin-coating: the sample holder was accelerated to 1500 rpm for 40 s and further increased to 2000 rpm for 20 s). The semiconductor layer (50 nm of pentacene or zinc phthalocyanine) is evaporated using the Evaporation Machine UNIVEX 350 (Leybold) and finally source and drain electrodes (60 nm Au or 70 nm Ca/30 nm Al) are evaporated in the glove-box using Leybold evaporation system. The device characteristics both output and transfer were measured in the glove-box (for pentacene and zinc phthalocyanine based devices) and in air (only for zinc phthalocyanine based devices) using Agilent E5273A 2 Channel Source / Monitor Unit. Based on the capacitance measurements of metal insulator metal (MIM) structures with different organic dielectrics, dielectric constant and capacitance per unit area for respective dielectric layers are presented in Table 2.



Figure 13 Chemical structure of organic semiconductors used for the device preparation, pentacene, phthalocyanine, P3HT (poly(3-hexylthiophene))

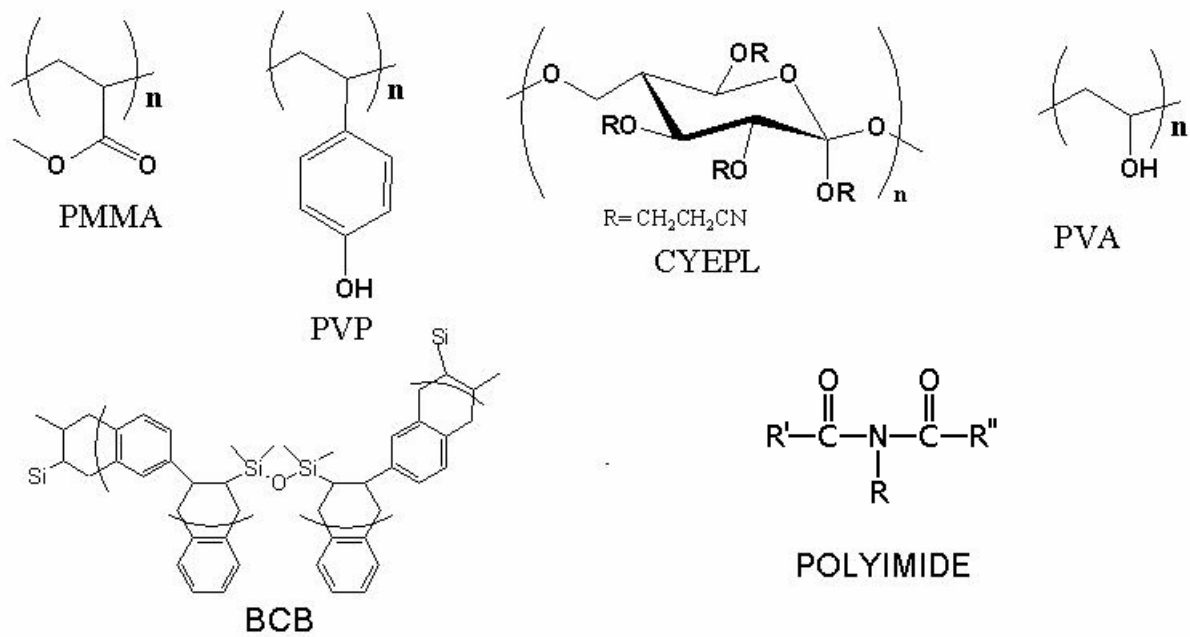


Figure 14 Chemical structure of organic dielectrics used for the systematic study, PMMA (polymethyl methacrylate), PVP (polyvinyl phenol), CyEPL (cyanoethylpullulan), PVA (polyvinyl alcohol), BCB (divinyltetramethyldisiloxanebis(benzocyclobutene)), polyimide

| Dielectric material | BCB | CYEPL | PI | PMMA | PVA | PVP |
|-----------------------------------|------|-------|-----|------|-----|-----|
| Dielectric constant | 2.7 | 12 | 3.4 | 3.5 | 8 | 4.5 |
| Capacitance [nF/cm ²] | 1.25 | 2.65 | 7.6 | 4.7 | 1.8 | 1.2 |

Table 2 Dielectric constants and capacitance per unit area of organic dielectrics used for device preparation

2.1.1 Devices with Pentacene

Among the organic semiconductors pentacene achieved the position of current benchmark material, exhibiting hole mobilities of approx. $6 \text{ cm}^2/\text{Vs}$ in organic field-effect transistors. [15] As shown in Figure 13 chemical structure of pentacene consists of 5 linearly-fused benzene rings. Pentacene has the appearance of a black powder or a purple thin film. For our OFET devices a 50 nm thick film of pentacene was deposited on top of dielectric layers. Pentacene films are grown at the rate of $0.2 - 0.3 \text{ \AA s}^{-1}$ at room temperature at a base vacuum of 10^{-6} mbar using Leybold Univex 350. Subsequently metal electrodes are deposited as source-drain electrodes. We have fabricated and characterized devices with various channel lengths, L , of 60 μm , 100 μm , 150 μm and a channel width of $W = 1 \text{ mm}$.

2.2.2 Devices with Zinc Phthalocyanine

Zinc phthalocyanine organic thin films of 50 nm were grown at the rate of $0.2 - 0.3 \text{ \AA s}^{-1}$ at room temperature at a base vacuum of 10^{-6} mbar using Leybold Univex 350. Devices with channel lengths, L , of 60 μm , 100 μm , 150 μm and a channel width of $W = 1-1.5 \text{ mm}$ were fabricated. The calculated electron and hole mobilities using the formula (4) for saturation regime are summarized for devices with $L = 60 \mu\text{m}$ and $W = 1.5 \text{ mm}$, giving a W/L ratio of 25, in Table 6, note that all the measurements are done in air.

2.2. Device fabrication and characterisation for FTIR measurements

For the investigation of the polymer/dielectric interface, devices with P3HT as a semiconductor in MIS (Metal-Insulator-Semiconductor)-structures as well as OFETs using SiO_2 as a dielectrics are employed and studied with the help of FTIR-spectrometer.

It is widely accepted that P3HT crystallize into layered domains at room temperature, with layers of conjugated backbones separated by layers of isolating alkyl chains. [25] The ability of P3HT to form highly ordered domains, however, depends on the degree of regioregularity of the polythiophenes' backbones. [26] In addition to the degree of order in the polymer film, the method of the film deposition greatly affects the field-effect mobility. [27] As reported in a previous paper by Kline et al. there is also a correlation between the molecular weight of P3HT and the device performance: the mobility of the device increases with the increase of

the molecular weight. [28] Further improvement in performance can be achieved by annealing the P3HT layer after deposition, which causes reduction of free volume in the layer and removal of residual solvent, thus leading to more compact and ordered films. [29][30]

Since charges in OFETs are transported mainly in a very thin layer adjacent to the gate insulator, the field effect mobility does not only depend on the purity and order of the organic layer but also on the quality and nature of the interface to the insulator. Silicon dioxide, SiO_2 , is widely used as a gate insulator in OFETs due to its excellent insulator properties and thermodynamically stability. However, the surface of SiO_2 exhibits a high density of hydroxyl groups which gives rise to a high surface free energy and, by this, to a tendency of forming strongly adhering layers of adsorbed contaminants from the ambient atmosphere. Therefore, the chemical treatment of SiO_2 with hexamethyldisilazane (HMDS) has been often used to improve the properties of field effect transistors with SiO_2 as the gate insulator. [31] [32] [27] [33] [34] [35] [36]. It is observed that silanization improves the field-effect mobility, concurrently with a significant reduction of the onset voltage and also improves stability in air. [31]

For the FTIR measurements the first criterion was to have a large area device in order to obtain a good signal. In the beginning the standard top contact / bottom gate structured transistors were built and characterised in the glove-box (Figure 15). Si/SiO_2 wafers are cleaned by putting into ultrasonic bath in Acetone for 15 min, and then in Methanol for 15 minutes and then in Hellmanex for 15 min at 70°C , finally washed with deionized water. Subsequently 50 nm thick gold electrodes are evaporated using the metal evaporator in the glove-box. After spin-coating P3HT at 4000 rpm the devices were annealed on the hotplate in the glove-box at 130°C for 5 minutes. The characterisation was made after transporting them to another glove-box immediately. The output characteristics and transfer curves are shown in the next chapter, illustrating a good working P3HT-transistor with very small hysteresis.

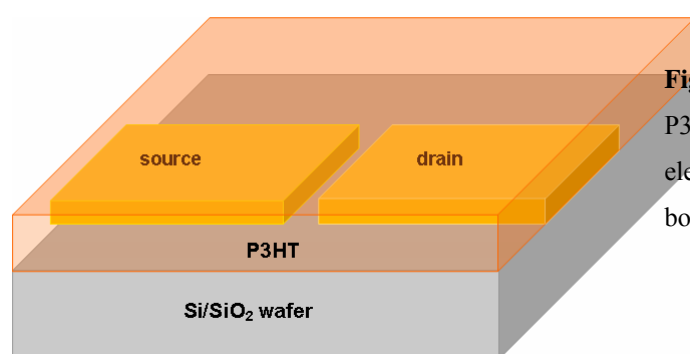


Figure 15 Device structure of transistors with P3HT as semiconductor and Au as source-drain electrodes on top of Si/SiO_2 wafer (bottom contact / bottom gate).

One of the devices fabricated in the same way but with large area interdigitated Au electrodes, structure illustrated in Figure 16, is short cut to obtain an MIS device. The contacts were taken from the Au- and highly doped silicon-electrodes using thin Au wires connected with the help of silver paint to the electrode surface.

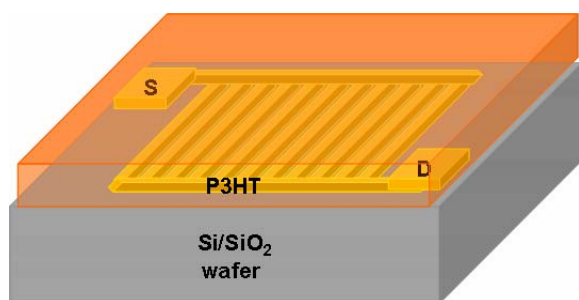


Figure 16 Device structure of (BG/TC) transistors with P3HT as semiconductor on top of Si/SiO₂ wafer (silicon acting as a gate electrode) with interdigitated Au source and drain electrodes (channel length $L=25\ \mu\text{m}$)

The devices used for the FTIR measurements were fabricated as described above only with an additional step of spincoating hexamethyldisilazane (HDMS) after cleaning the Si/SiO₂ substrates to achieve the passivation of the surface.

2.3. FTIR measurements

The devices used for the infrared spectroscopy are prepared and measured as explained in the previous chapter 2.2. The device characteristics (the results of both output and transfer measurements for the transistors and capacitance measurement for the MIS-structure) are also presented in the same chapter.

For the infrared spectroscopy measurements a Bruker IFS 66/S FTIR spectrometer in transmission mode is used. The spectrometer is equipped with a KBr beamsplitter and a mercury-cadmium-telluride (MCT) detector, which is cooled with liquid nitrogen down to 77 K. After the samples are placed into the sample chamber the chamber is purged with nitrogen for minimum 30 minutes before starting with the measurement.

To obtain the voltage induced spectroscopy results, the device is mounted into the sample holder and contacts are taken with thin Au-wires and silver paint. A simple programme in the OPUS software is used to trigger and control the scan parameters and the applied voltage, which is amplified by an operational amplifier up to 30 times the original output value of the four channel digital delay / pulse generator. The method of the measurement is illustrated in Figure 17: at time $t = 0$, a certain voltage $V \neq 0$ is applied via the delay / pulse generator to the device, after 2 seconds ($t = 2$ s): the spectrometer starts with scanning, scans for the next 16 seconds (32 scans), stops at $t = 18$ s and saves the spectrum. For simplicity the result of this scan with $V \neq 0$ will be referred to ON-spectrum in the following text. At $t = 20$ s the applied voltage is set back to 0, $V = 0$, and at $t = 22$ s the spectrometer starts scanning for the next 16 s and stops at $t = 38$ s and saves the result, OFF-spectrum. At $t = 40$ s a new 40 cycle starts providing the ON-spectrum-2 and OFF-spectrum-2. After 250 cycles the measurement is finished and the difference spectrum is calculated from the obtained ON- and OFF-spectra:

$$spectrum_{difference} = \sum_{i=1}^{250} spectrum_{OFF,i} / \sum_{i=1}^{250} spectrum_{ON,i}$$

Figure 30 in the next chapter shows the result of an FTIR measurement done using the method explained above, to the P3HT MIS structure ($V = 5$ V, 10 V, 15 V, 20 V, 25 V, 30 V) are applied and the calculated difference spectrum is plotted for each voltage. For comparison the spectrum of chemically doped P3HT is also taken. First P3HT from solution is spin-coated on Si/SiO₂ substrates and then a 1-minute-scan in the transmission mode is made. Subsequently P3HT coated Si/SiO₂ substrate is taken out of the spectrometer and doped with

I₂-vapor. The spectrum via 1-minute-scan is taken and is divided by the previous spectrum; the result is plotted in Figure 31. Also here the polaronic band and the vibrational bands are observed.

The difference spectra of a P3HT transistor is obtained, where the voltage between source and drain is kept constant at $V_d = -40 V$, the gate voltage V_g , however, alternates between 0 and a nonzero value. Similar to the findings of the measurement of the MIS-structure the spectra show two voltage induced features, namely the polaronic band and the IR/V bands, again the absorption increasing with the gate voltage V_g .

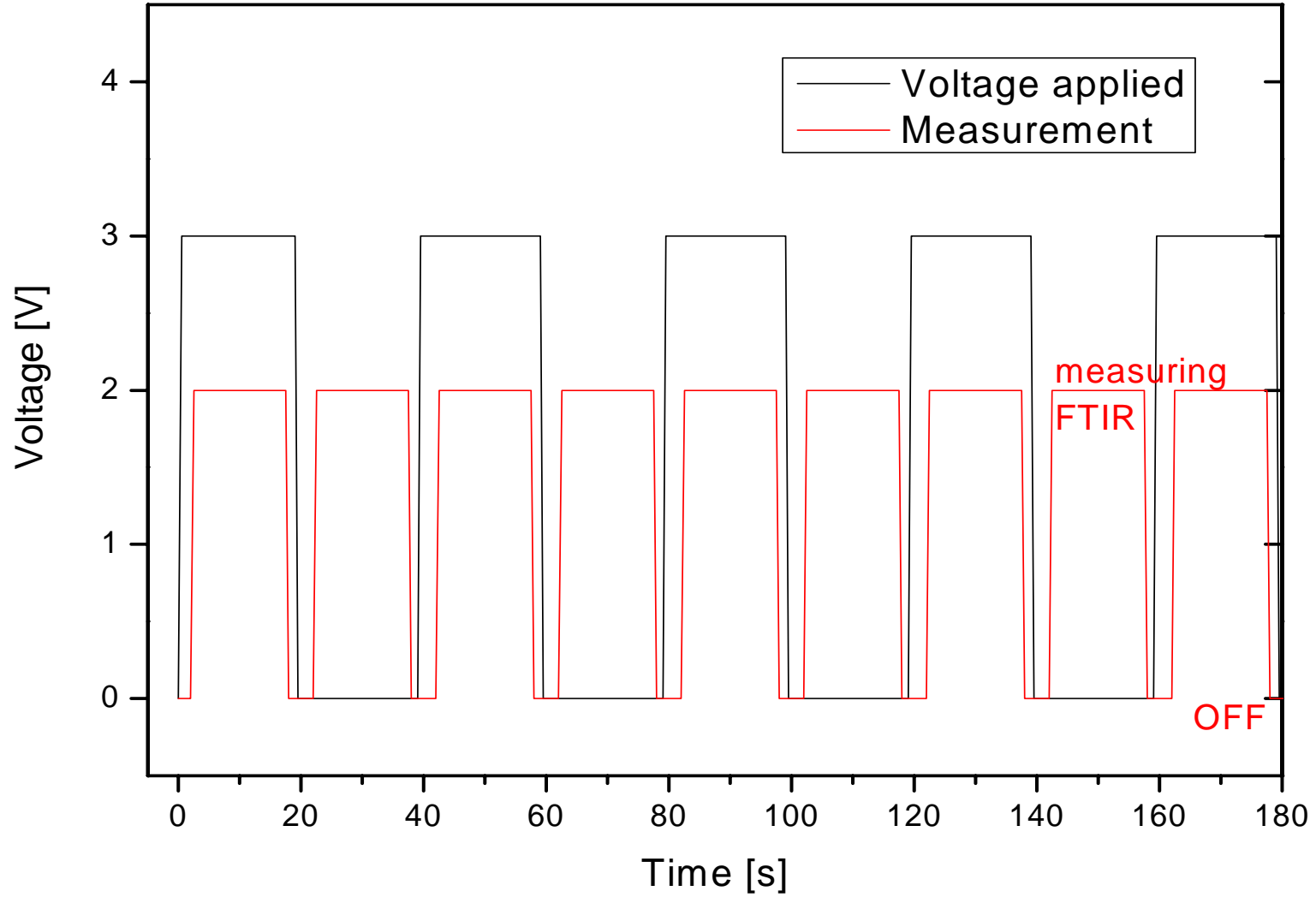


Figure 17 The evolution of FTIR measurement: applied gate voltage and scanning versus time

2.4. List of Instruments

- 2 Channel (High Power / Medium Power) Source Monitor Unit E5273A (Agilent Technologies)
- 80 MHz Function / Arbitrary Waveform Generator (Agilent Technologies)
- Precision LCR-Meter 20Hz – 1 MHz 4284 A (Hewlett Packard)
- Bruker IFS 66/S FTIR spectrometer
- Aquatherm H₂O cooling system
- Stanford Research Systems, Inc. DG 535 Four Channel Digital Delay / Pulse Generator
- Keithley 2400 Sourcemeter...
- Digital Multimeter 236 Source Measure Unit (Keithley)
- Glovebox MB 150B-G / MB 200B (MBraun)
- Evaporation Machine UNIVEX350 (Leybold)
- Evaporation Control AS 053 (Leybold)
- Evaporation Control IL820 (Intellemetrics)
- Spincoater Model P6700 Series (Speciality Coating Systems Inc.)
- Ultrasonic S 10H Elmasonic (Elma)
- Ultrasonic 150S (Sonomatic)
- Stirrer RH Basic 2 (IKA) IKAMAG RH
- 4100 Digital Multimeter / Switch System Integral Series (Keithley)
- Turbo Pump / Vacuum Turbo Cube (Pfeiffer)

2.5. List of Materials

In Table 3 you can see a list of all chemical substances and metals used for device fabrication.

| Substance | Chem. structure | M / g mol ⁻¹ | Company |
|---------------------|----------------------------------|-------------------------|--------------------|
| Aceton | C ₃ H ₆ O | 58.08 | J. C. Baker |
| Isopropanol | C ₃ H ₈ O | 60.10 | J. C. Baker |
| n-Butanol | C ₄ H ₁₀ O | 74.12 | J. C. Baker |
| Hellmanex | - | - | Hellma |
| Chlorbenzene | C ₆ H ₅ Cl | 112.56 | J. C. Baker |
| Pentacene | Fig 11 | 278.4 | Sigma Aldrich |
| Zinc Phthalocyanine | Fig 11 | | Sigma Aldrich |
| P3HT | Fig 11 | | Merck Chemicals |
| BCB [Cyclotene™] | Fig 12 | | Dow Chemicals |
| CyEPL | Fig 12 | | Shin-Etsu Chemical |
| PI | Fig 12 | | Polycera |
| PMMA | Fig 12 | | Sigma Aldrich |
| PVA [Mowiol® 40-88] | Fig 12 | | Sigma Aldrich |
| PVP | Fig 12 | | Sigma Aldrich |
| Silver Paint | Ag | 107.87 | Sigma Aldrich |
| Calcium | Ca | 40.08 | |
| Gold | Au | 196.96 | Oegussa |
| Aluminium | Al | 26.98 | Oegussa |
| Lithiumfluoride | LiF | 25.94 | Sigma Aldrich |
| Iodine | I ₂ | 126.9 | |

Table 3 List of all materials used for the experiments

3. Results and Discussion

To investigate the correlation between the dielectric material and ambipolarity a systematic study of transistors is done using two different semiconductors, namely pentacene and phthalocyanine, combining them with 6 different organic dielectrics, namely BCB, CyEPL, PI, PMMA, PVA, PVP and two different source- and drain-electrode-metals, namely Au and Ca/Al. For pentacene devices the calculated electron and hole mobilities using the formula (4) for saturation regime are summarized for only devices with $L = 60 \mu\text{m}$ and $W = 1.5 \text{ mm}$, giving a W/L ratio of 25, in Table 4. Rest of the devices with different W/L is not described here simply.

The choice of the dielectrics plays a crucial role for the device performance [16] and also the interface between the organic semiconductor and the gate dielectric. [17][18][19].

In our study all of the pentacene devices showed ambipolar transport with the hole mobility being in general 3-4 orders of magnitude higher than the electron mobility (Table 4). Figure 18 and Figure 19 illustrate the transfer characteristics of the devices, which were used for mobility calculations. In Figure 20 one can see the transfer characteristics of the devices with the same structure but this time with Ca/Al electrodes instead of Au. Using Ca/Al electrodes the devices with BCB, PVA, PI were not showing transistor properties and no ambipolar transport was observed as summarized in Table 5.

| | HOLE MOBILITY [cm^2/Vs] | ELECTRON MOBILITY [cm^2/Vs] |
|-------|--|--|
| BCB | 2×10^{-4} | 8×10^{-7} |
| CYEPL | 7×10^{-2} | 5×10^{-6} |
| PI | 1 | 9×10^{-4} |
| PMMA | 7×10^{-2} | 9×10^{-6} |
| PVA | 7×10^{-2} | 2×10^{-2} |
| PVP | 1×10^{-1} | 1×10^{-5} |

Table 4 Mobility values calculated for pentacene transistors with various organic dielectrics, using Au source- and drain-electrodes, $L = 60 \mu\text{m}$, $W = 1.5 \text{ mm}$

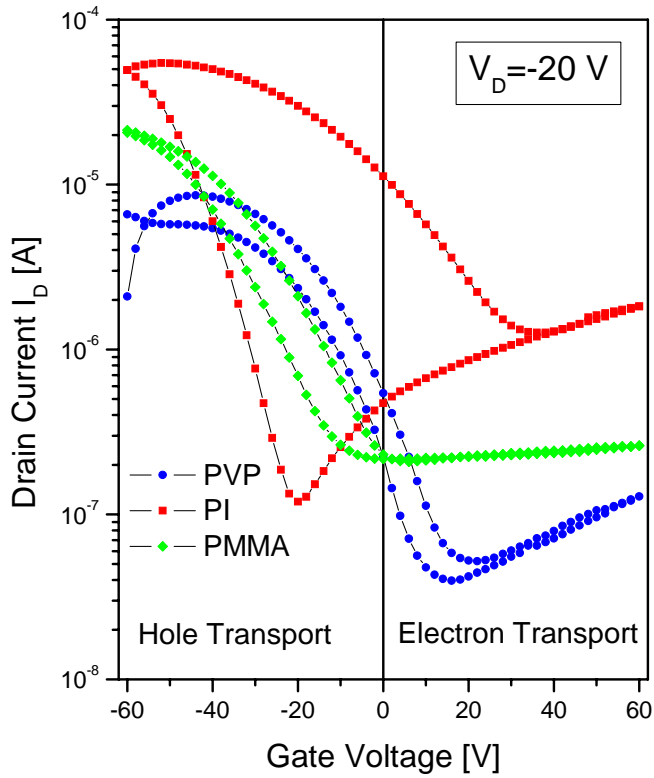


Figure 18 Transfer characteristics of pentacene OFETs with different dielectrics (PMMA (polymethyl methacrylate), PVP (polyvinyl phenol), polyimide) and Au as source-drain electrodes. Ambipolar transport is evident in OFETs with PVP and PI gate dielectrics. Significant hysteresis is observed in these devices.

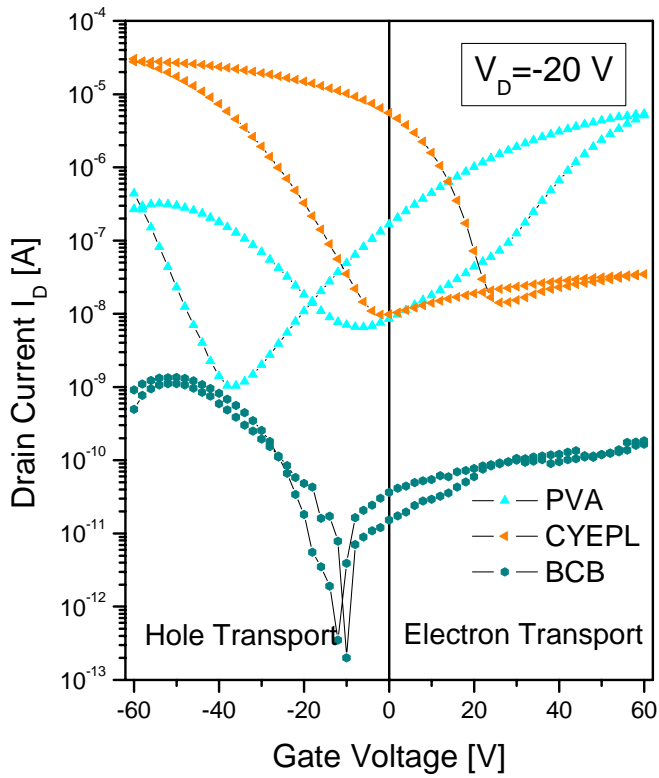


Figure 19. Transfer characteristics of pentacene OFETs with different dielectrics (CyEPL (Cyanoethylpullulan), PVA (polyvinyl alcohol), BCB (divinyltetramethyldisiloxane bis(benzocyclobutene))). Ambipolar transport is observed in OFETs with PVA and CyEPL dielectrics.

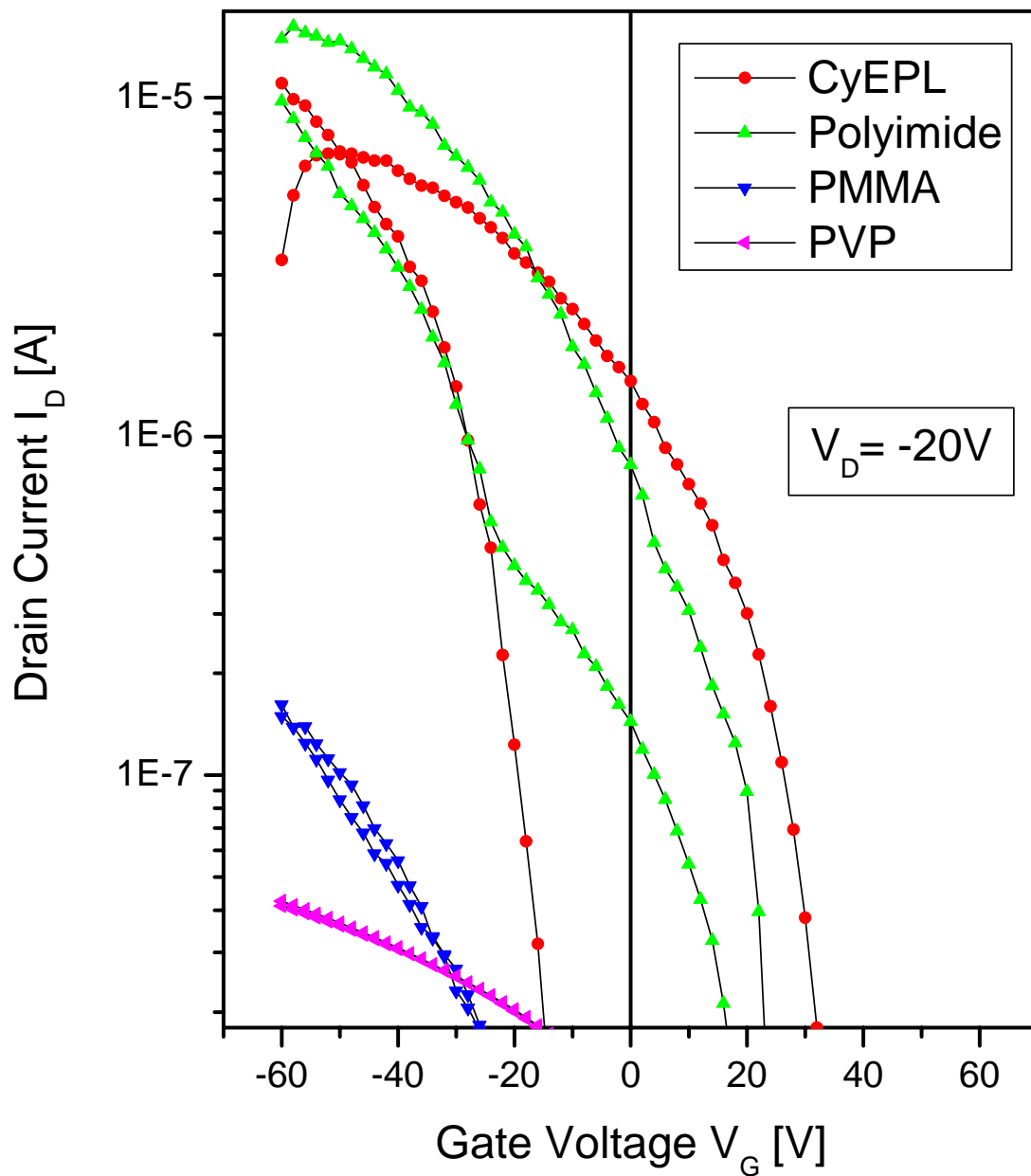


Figure 20 Transfer characteristics of pentacene transistors with Ca/Al electrodes using various dielectrics (PMMA (polymethyl methacrylate), PVP (polyvinyl phenol), polyimide (PI), CyEPL (cyanoethylpullulan))

| | HOLE MOBILITY [cm^2/Vs] | ELECTRON MOBILITY [cm^2/Vs] |
|-------|---|---|
| CYEPL | 3.5×10^{-4} | not active |
| PMMA | 8.5×10^{-4} | not active |
| PVP | 3.4×10^{-1} | not active |

Table 5 Mobility values calculated for pentacene transistors with various organic dielectrics, using Ca/Al source- and drain-electrodes, $L = 60 \mu\text{m}$, $W = 1.5 \text{ mm}$

Phthalocyanines (Pcs) as organic semiconductors, chemical structure illustrated in Figure 13, have been studied widely owing to their intense optical absorptions and excellent optoelectronic properties [48][50]. Bao et al. fabricated OFETs employing copper phthalocyanine (CuPc) functioning as p-channel accumulation-mode devices with a mobility of $0.02 \text{ cm}^2\text{V}^{-1}\text{s}^{-1}$. [20][21] The charge carrier mobility of such devices is strongly dependent on the morphology of the semiconducting thin film. For sandwich structures (using copper phthalocyanine and cobalt phthalocyanine together) mobilities up to $0.11 \text{ cm}^2\text{V}^{-1}\text{s}^{-1}$ for OFETs are reported for metallophthalocyanines[22][3]. Ambipolar transport was observed in Pc-based OFETs by Bao and co-workers [23].

It is known that for zinc phthalocyanine films, as with other p-type metallophthalocyanines (MPcs), oxygen molecules can diffuse into the film and act as acceptors leading to an increase in the concentration of positive charge carriers. Oxygen molecules present in the ZnPc films not only play the role of acceptor dopant but also create localised charge carrier states, connected with oxygen occupying space between grains, which lead to polarisation effects within the lower frequency range [24]. *I-V* measurements are done for top gate/bottom contact ZnPc transistors in air and in the glove-box showing a higher conductivity in air due to the oxygen doping in agreement with the conclusion of cited paper above. The comparison of two transfer curves for the same transistor measured in air and in the glove-box is illustrated in Figure 21.

| | HOLE MOBILITY [cm^2/Vs] | ELECTRON MOBILITY [cm^2/Vs] |
|-------|---|---|
| BCB | 2.3×10^{-4} | not active |
| CYEPL | 1.1×10^{-3} | 1.6×10^{-5} |
| PI | 1.9×10^{-4} | not active |
| PMMA | 1.5×10^{-3} | not active |
| PVA | 2.2×10^{-3} | not active |
| PVP | 3.4×10^{-4} | not active |

Table 6 Mobility values calculated for zinc phthalocyanine transistors with various organic dielectrics using Au source- and drain-electrodes:

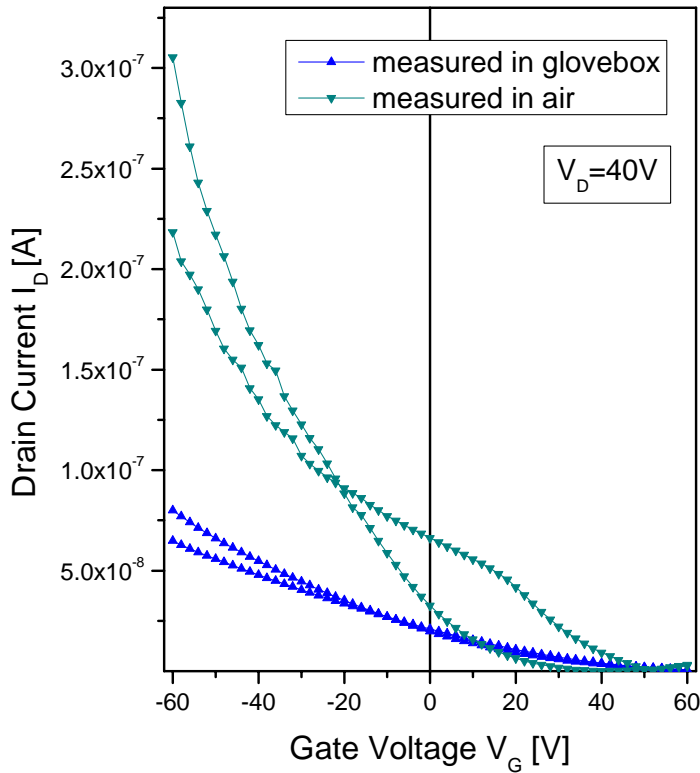


Figure 21 Comparison of transfer characteristics of a zinc phthalocyanine transistor with polyimide as dielectric measured under Argon atmosphere and in air.

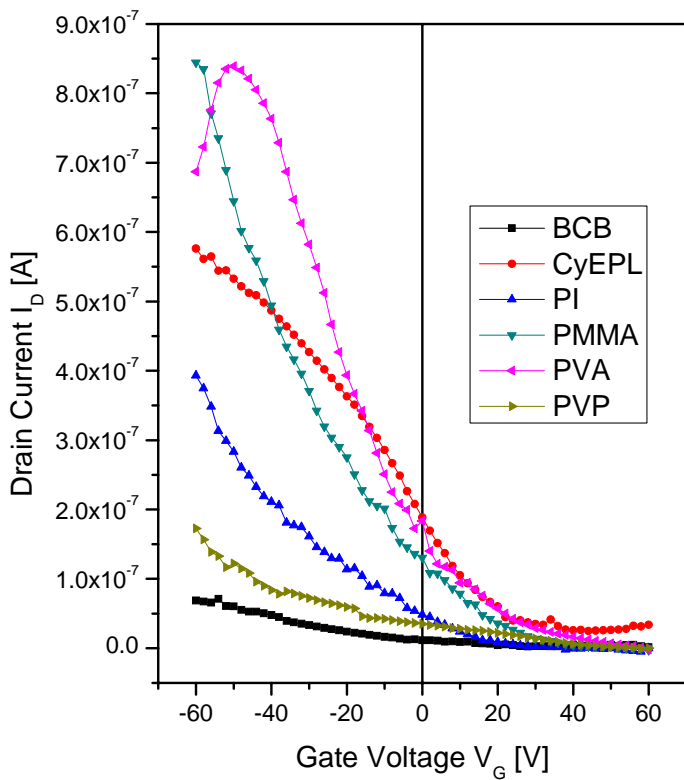


Figure 22 Transfer characteristics measured in Ar atmosphere for phthalocyanine OFETs with different dielectrics (CyEPL (Cyanoeethylpullulan), PVA (polyvinyl alcohol), BCB (divinyltetramethylsiloxane bis(benzocyclobutene)), PMMA (polymethyl methacrylate), PVP (polyvinyl phenol), PI (polyimide)). Only the device using CyEPL shows ambipolar transport.

In our study only the devices with CyEPL as dielectric showed ambipolar transport with the hole mobility being 1-2 orders of magnitude higher than the electron mobility. The results are in agreement with the work of Mizuno and his co-workers [80]. Figure 22 presents the transfer characteristics of the devices, which were used for mobility calculations. The devices where Ca/Al electrodes were used instead of Au didn't have transistor properties.

For the FTIR measurements, in the beginning, transistors with P3HT as semiconductor are produced on top of Si/SiO₂ substrates. The output characteristics in Figure 23 are showing a well defined saturation, where the saturated drain current I_d is 5×10^{-7} A for $V_d = -30$ V and Figure 24 shows the transfer characteristics of the same device. Figure 25 shows the results of the capacitance measurements for the MIS structure done with an LCR meter in the FTIR-spectrometer under N₂ atmosphere. The capacitance measurements of the large area MIS structure with interdigitated Au-electrodes show not only hole transport but also show signatures of electron transport (Figure 25).

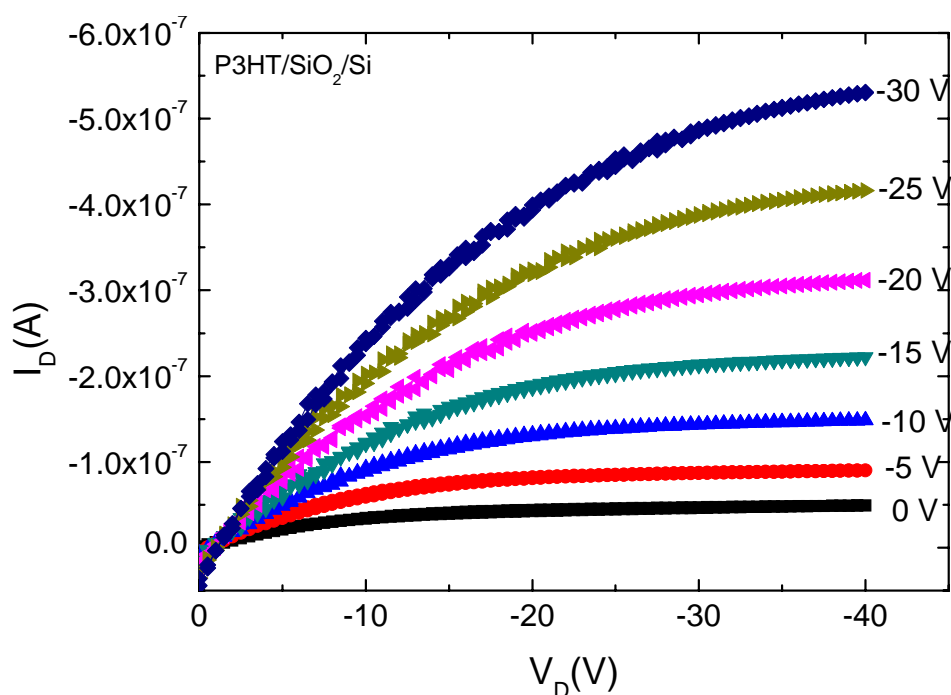


Figure 23 Output characteristics of P3HT-OFETs scheme as shown in Figure 15 indicating hole-enhanced mode. Applied gate voltages are indicated for respective curves.

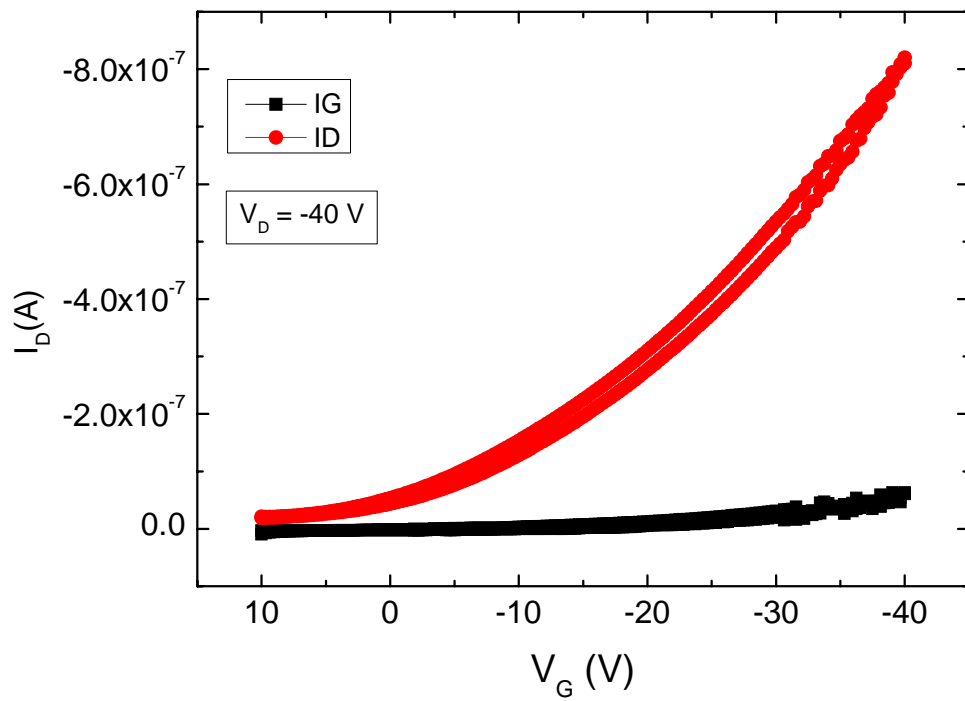


Figure 24 Transfer characteristics of P3HT OFETs scheme as shown in Figure 15 for drain voltage of -40 V.

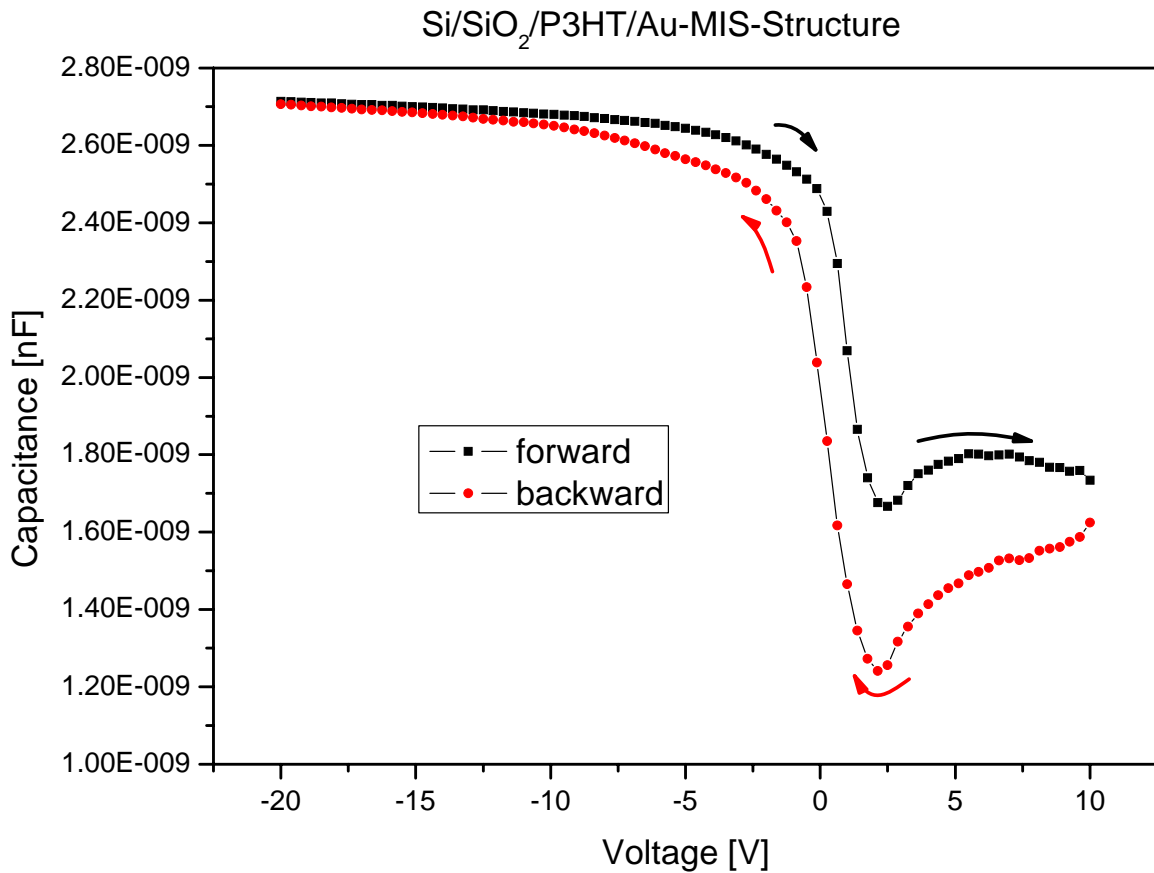


Figure 25 Capacitance measurements of Si/SiO₂/P3HT/Au-MIS-Structure

Large area P3HT-transistors with interdigitated Au electrodes are built on top of Si/SiO₂ substrates (Figure 16). In the output characteristics, measured in the glove-box under N₂ atmosphere a not so well-defined saturation is observed (Figure 26), but when the measurement is repeated in the spectrometer under N₂ atmosphere after transport through air, the saturation behaviour is disappeared and the I - V curves show linear dependency and I_d values are quenched down to the half of the original value although an increase is expected due to the doping of P3HT with oxygen (Figure 27). Also in transfer characteristics in Figures 28 and 29 a similar increase in the current is observed.

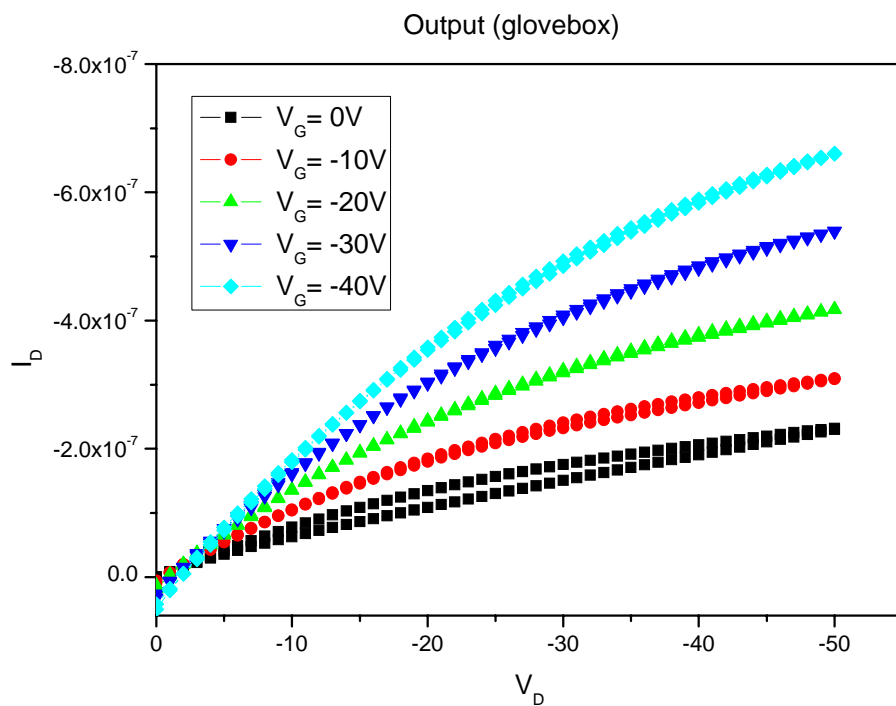


Figure 26 Output characteristics of P3HT-transistor on Si/SiO₂ with interdigitated electrodes, taken in the glovebox under N₂ atmosphere

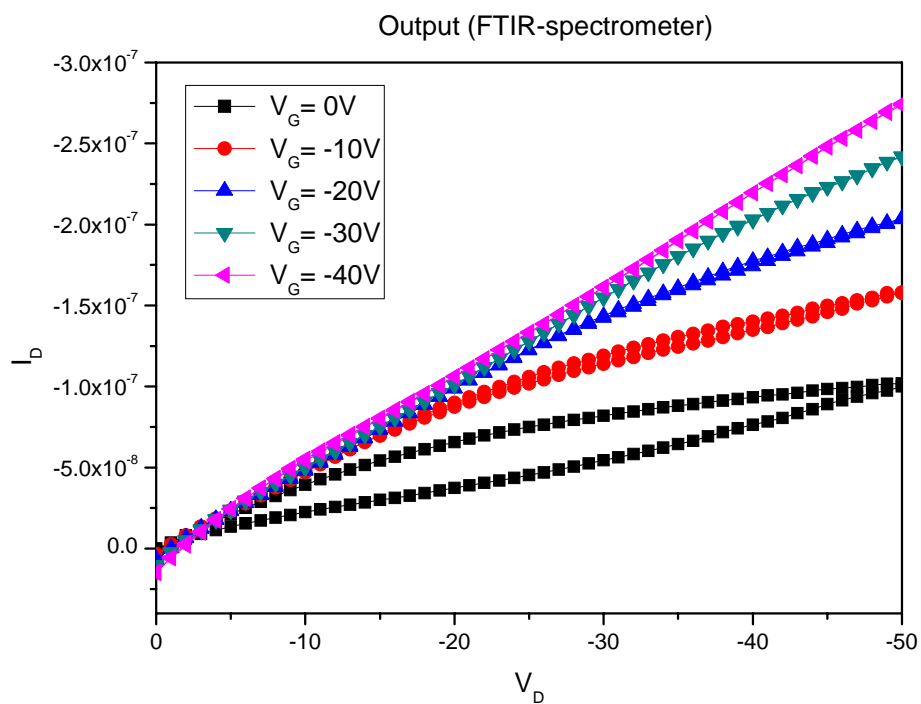


Figure 27 Output characteristics of P3HT-transistor on Si/SiO₂ with interdigitated electrodes, taken in the FTIR-Spectrometer under N₂ atmosphere after transport through air

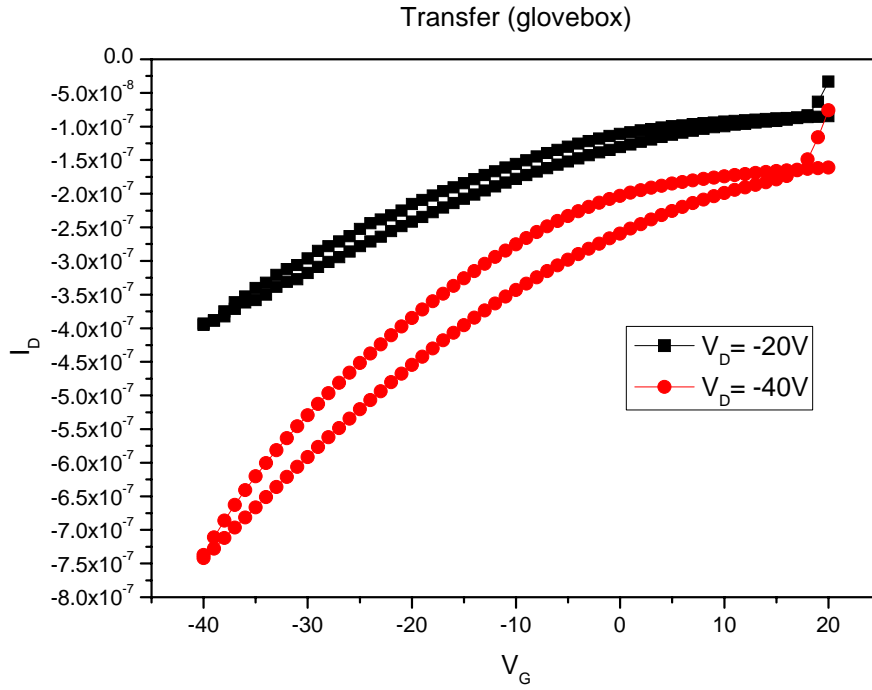


Figure 28 Transfer characteristics of P3HT-transistor on Si/SiO₂ with interdigitated electrodes, taken in the glovebox under N₂ atmosphere

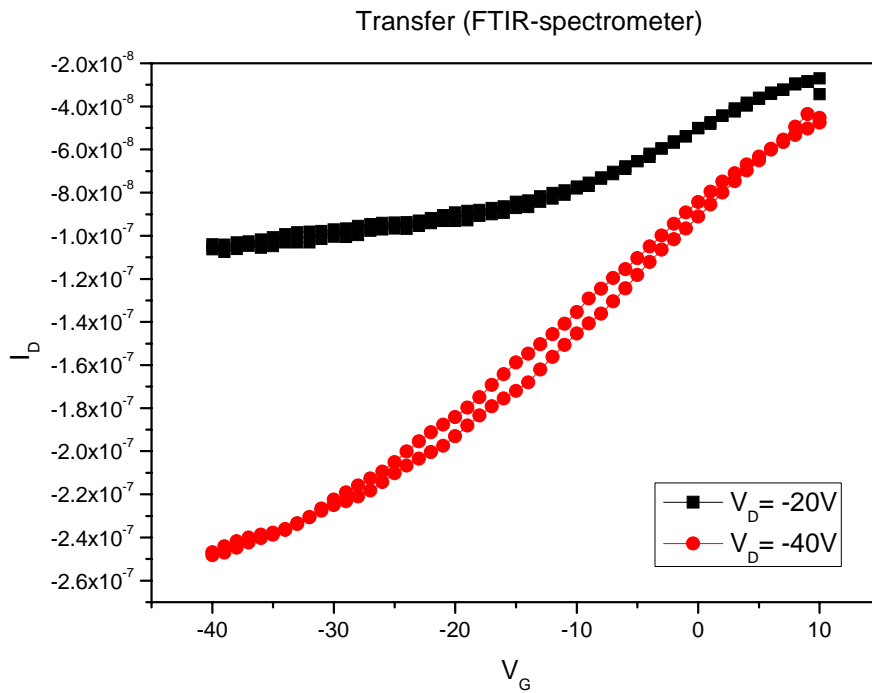


Figure 29 Transfer characteristics of P3HT-transistor on Si/SiO₂ with interdigitated electrodes, taken in the FTIR-Spectrometer under N₂ atmosphere after transport through air

In Figure 30, the FTIR measurements done with the P3HT-MIS structure applying different voltages show two voltage-induced features: (i) sharp resonances in the 1000-1500 cm^{-1} region, and (ii) a broad band centered around 3000 cm^{-1} . A gradual development of these features with increasing gate voltage V_{GS} suggests that they are intimately related to the formation of charge accumulation layer in P3HT. Sharp resonances in the 1000-1500 cm^{-1} range result from the IR active vibrational modes (IRAVs), i.e., Raman modes made IR active by distortions of the polymer backbone caused by the self-localized charges [40]. The broad absorption band centered around 3000 cm^{-1} is usually ascribed to a midgap state of polaron or bipolaron associated with the local relaxation of the lattice around the doped charge [40][11]. Whether this absorption is due to polaron or bipolaron is still under investigation [41][42]. To make a comparison the FTIR spectrum of chemically doped P3HT is taken and presented in Figure 31. Figure 32 illustrates the difference spectrum for the P3HT MIS structure at $V = -30 \text{ V}$ along with the data for chemically doped P3HT, where the frequencies of the IRAV modes are in agreement with the vibrational resonances found in chemically doped P3HT. The results are also in agreement with experiments done by Li et al. where FET devices in bottom geometry are produced using P3HT and TiO_2 . The structure and characteristics of the devices are shown in Figure 34 and the results of the FTIR measurements and comparison of chemical and voltage induced doping are presented in Figure 35 [11]. For the P3HT transistors produced in our labs, again all spectra uncover spectroscopic fingerprints of electrostatic doping: IRAV modes in the 1000-1500 cm^{-1} range and a polaronic band at 3000 cm^{-1} (Figure 33). Again compared to the previous work done by Li et al., the results are in conformity [11].

As a next step the ATR-FTIR spectroscopy of organic dielectric/organic semiconductor interface is possible and a better understanding of the mechanism of ambipolar transport should be achieved due to results of ATR experiments. The problems we were facing during the ATR measurements of devices with organic dielectrics was the limited reducibility of insulator thickness, and poor reproducibility of working large area transistors on top of Germanium ATR-crystals with sufficient good FTIR signal to make a conclusion about the ambipolarity.

Si/SiO₂/P3HT/Au-MIS-Structure

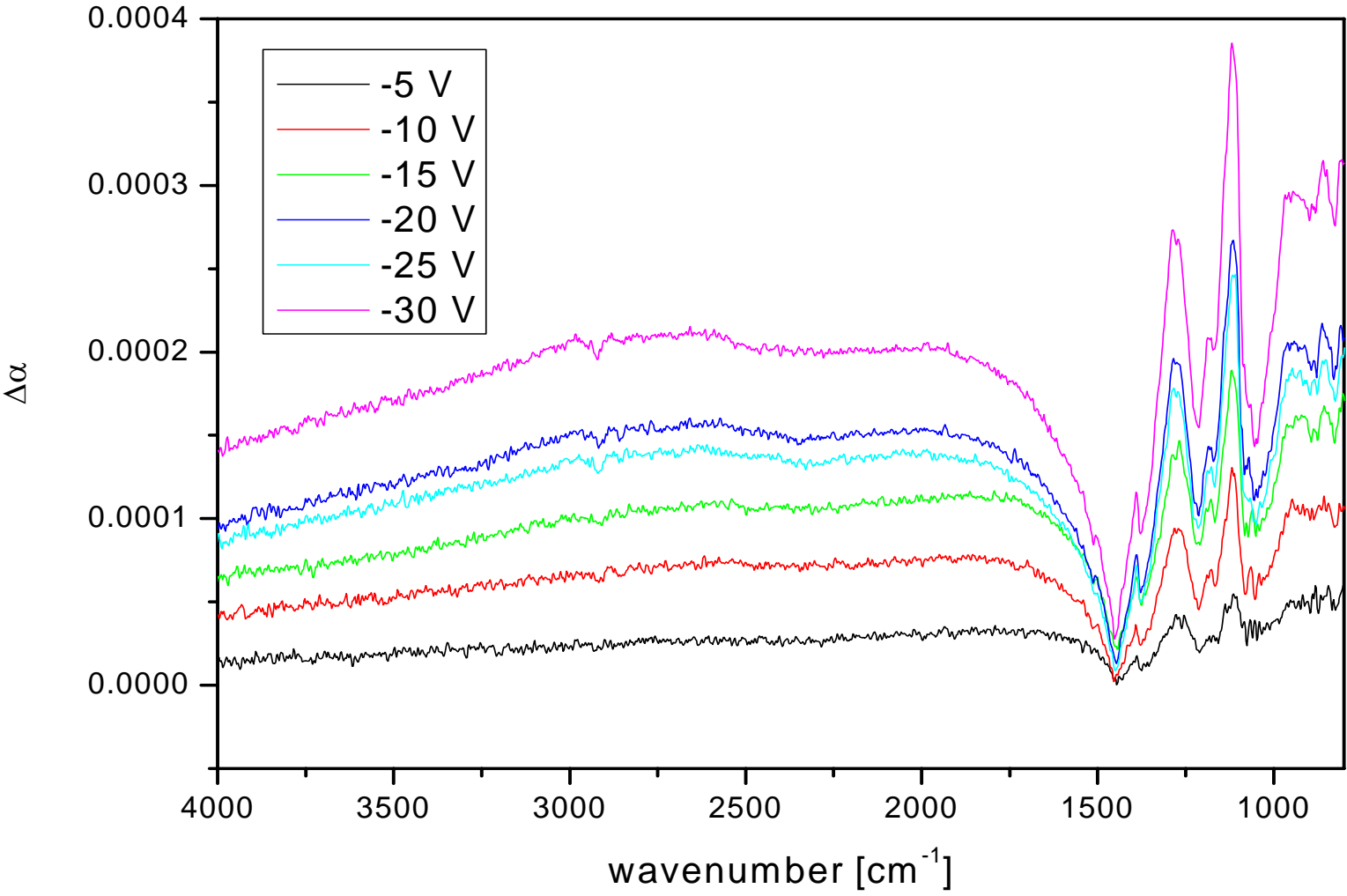


Figure 30 Difference spectrum of MIS structure P3HT on Si/SiO₂

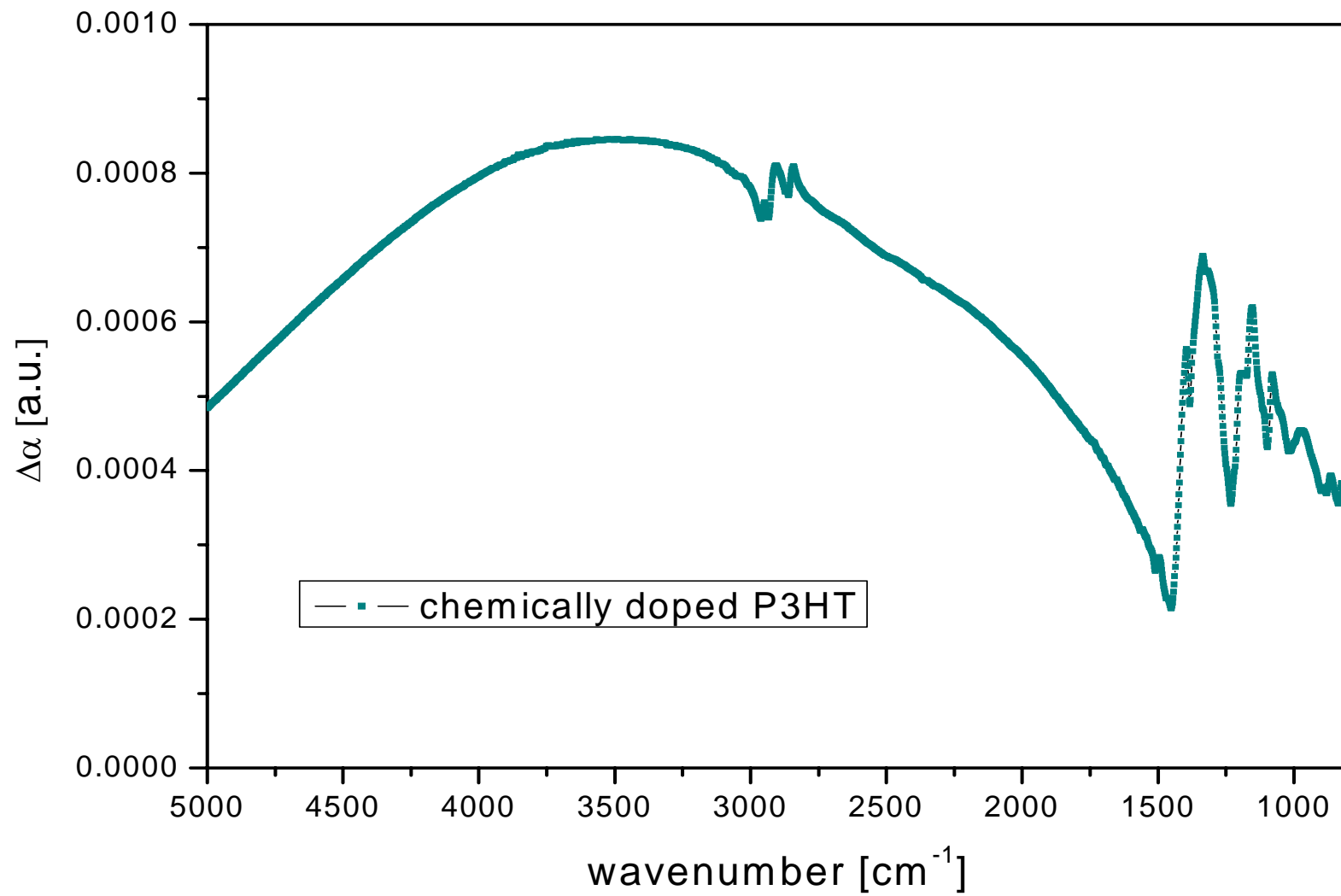


Figure 31 Absorption spectrum of chemically doped P3HT

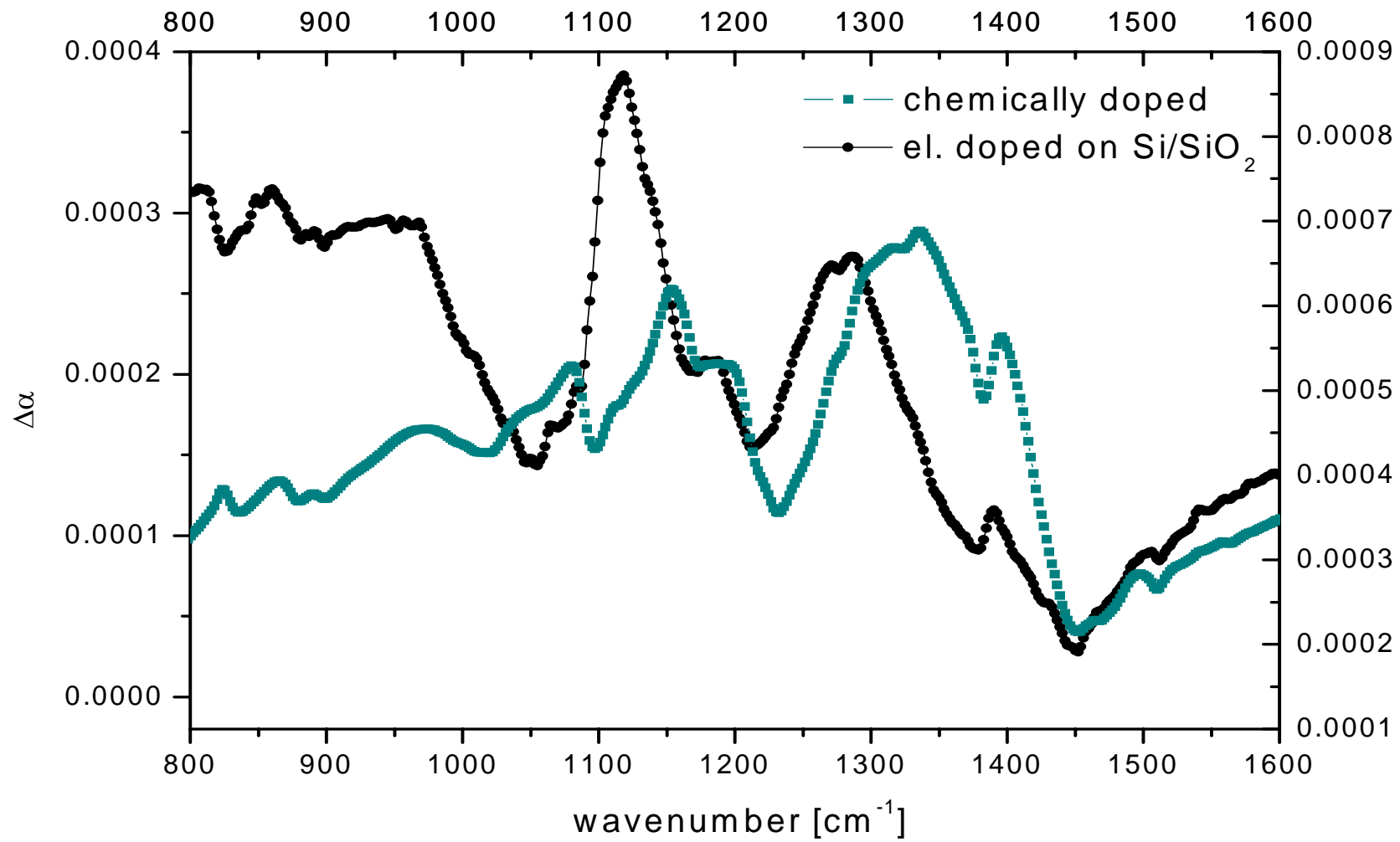


Figure 32 Comparison of chemically doped P3HT with voltage induced absorption spectrum in the IRAV-bands region (800-1600 cm⁻¹)

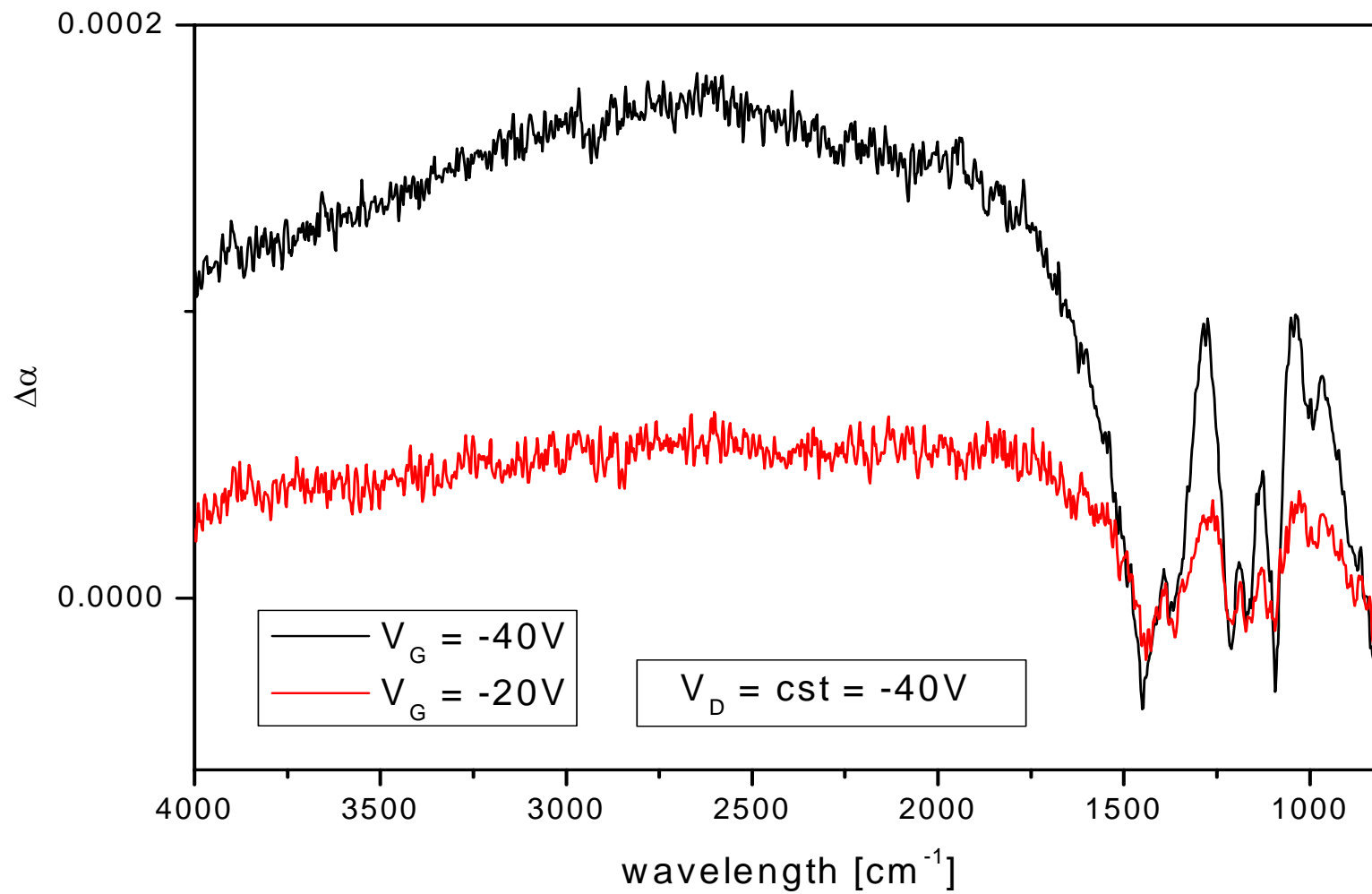


Figure 33 Difference spectrum of P3HT-transistor on Si/SiO₂

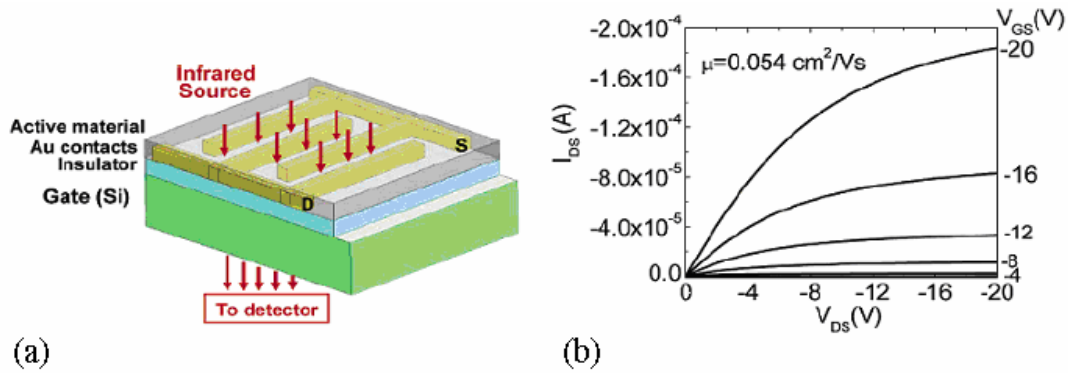


Figure 34 (a) Schematic of a FET device in the bottom contact geometry for infrared characterization of charge injection. The active material in the FET devices is P3HT. (b) The I - V curve of a representative TiO_2 -based FET (Figure taken from [11])

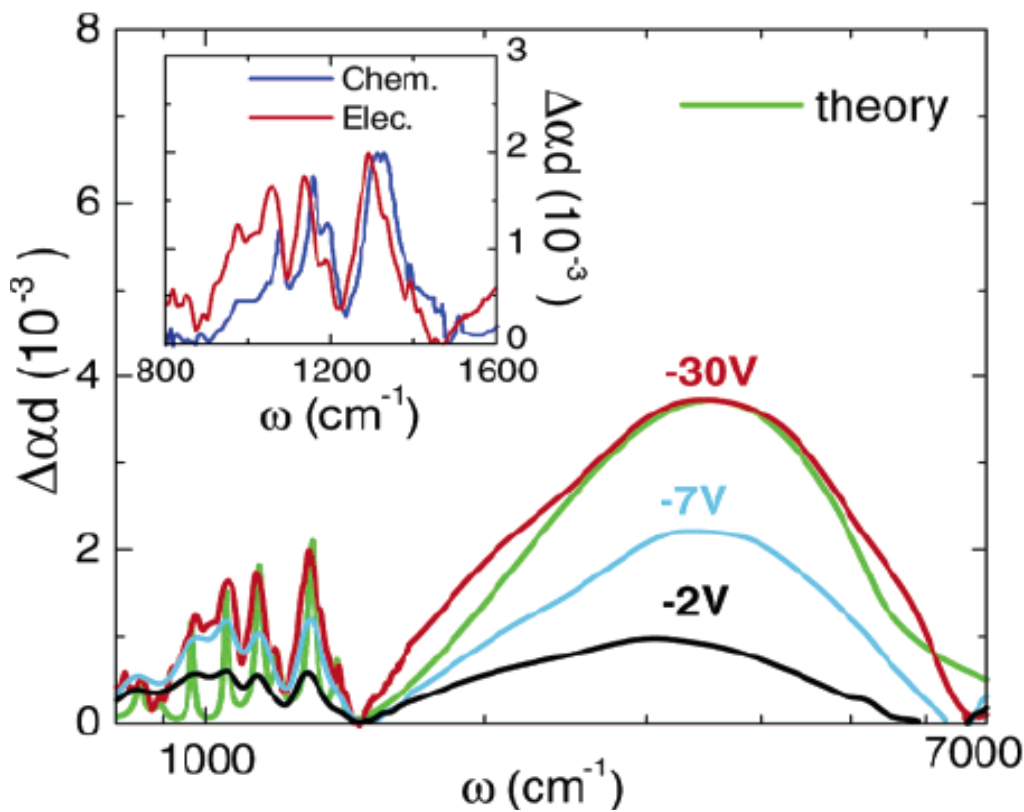


Figure 35 The voltage-induced absorption spectra $\Delta\alpha_d$ for the P3HT layer under applied gate voltages V_{gs} in a TiO_2 -based device. The green curve is a theoretical modelling of the experimental spectrum. (inset) $\Delta\alpha_d$ spectrum for a representative TiO_2 -based device at $V_{gs} = -30 \text{ V}$ along with the data for chemically doped P3HT [11]. The latter is the difference spectrum between the absorption of chemically doped P3HT with 1 mol % PF_6^- and that of pure P3HT [11] scaled by a factor of 4×10^5 . (Figure taken from [11])

References

- [1] A. Tsumura, H. Koezuka and T. Ando, *Appl. Phys. Lett.* **1986**, 49, 1210
- [2] A. Facchetti, M. H. Yoon, T. J. Marks, *Adv. Mater.* **2005**, 17, 1705
- [3] Th. B. Singh, N. S. Sariciftci, *Annu. Rev. Mater. Res.* **2006**, 36, 199-230
- [4] S. M. Sze, *Semiconductor Devices, Physics and Technology*, **2001**, 2, 169-220
- [5] P. Stadler, Hysteresis in Bio-Organic Field-Effect Transistors, *Diploma Thesis at Linz Institute of Organic Solar Cells*, **2006**
- [6] B. Singh, P. Senkarabacak, N. S. Sariciftci, A. Tanda, C. Lackner, R. Hagelauer, G. Horowitz, *Appl. Phys. Lett.* **2006**, 89, 033512-1
- [7] X. Peng, G. Horowitz, D. Fichou, F. Garnier, *Appl. Phys. Lett.* **1990**, 57, 2013
- [8] H. Klauk, M. Halik, U. Zschieschang, G. Schmid, W. Radlik, W. Weber, *J. Appl. Phys.* **2002**, 92, 5259
- [9] J. Veres, S. D. Ogier, S. W. Leeming, D. C. Cupertino, S. M. Khaffaf, *Adv. Funct. Mater.* **2003**, 13, 199
- [10] L.-L. Chua, J. Zaumseil, J.-F. Chang, E. C.-W. Ou, P. K.-H. Ho, H. Sirringhaus, R. H. Friend, *Nature* **2005**, 434, 194
- [11] Z. Q. Li, G. M. Wang, N. Sai, D. Moses, M. C. Martin, M. Di Ventra, A.J. Heeger, and D. N. Basov, *Nano Letters* **2006**, 6 (2): 224-228
- [12] T. J. Johnson, G. Zachmann, *Introduction to Step Scan Spectroscopy*, Bruker Optik GmbH, Germany
- [13] P. R. Griffiths, J. A. de Haseth, *Fourier Transform Infrared Spectroscopy*, (J. Wiley&Sons, Inc., New York, 1986)

- [14] Brian C. Smith, *Fundamentals of Fourier Transform Infrared Spectroscopy*, CRC press, Boca Raton, **1996** (for further information: Keck-II, Interdisciplinary Surface Science Center, Northwestern University webpage)
- [15] T. W. Kelley, D. V. Muyres, P. F. Baude, T. P. Smith, T. D. Jones, *Mater. Res. Soc. Symp. Proc.* **2003**, 771:L6.5.1
- [16] Th. B. Singh, N. Marjanovic, P. Stadler, M. Auinger, G. J. Matt, S. Günes, N. S. Sariciftci, R. Schwödiauer, S. Bauer, *J. Appl Phys.* **2005**, 97, 083 714
- [17] R. G. Keppler, *Phys. Rev.* **1960**, 119, 1266
- [18] Th. B. Singh, S. Günes, N. Marjanovic, R. Menon, N. S. Sariciftci, *J. Appl. Phys.* **2005**, 97, 114 508
- [19] Th. B. Singh, F. Maghdedi, S. Günes, N. Marjanovic, G. Horowitz, P. Lang, S. Bauer, N. S. Sariciftci, *Adv. Mater.* **2005**, 17, 2315-2320
- [20] Z. Bao, A. J. Lovinger, A. Dodabalapur, *Appl. Phys. Lett.* **1996**, 69, 3066
- [21] Z. Bao, A. J. Lovinger, A. Dodabalapur, *Adv. Mater.* **1997**, 9, 42
- [22] J. Zhang, J. Wang, H. Wang, D. Yan, *Appl. Phys. Lett.* **2004**, 84, 142
- [23] J. Locklin, K. Shinbo, K. Onishi, F. Kaneko, Z. Bao, C. Advincula, *Chem. Mater.* **2003**, 15, 1404
- [24] G. Jarosz, P. D. Quinn, N. Stephan, L. Brehmer, *Thin Solid Films* **2005**, 474, 301
- [25] T. J. Prosa, M. J. Winokur, J. Moulton, P. Smith, A. J. Heeger, *Macromolecules* **1992**, 25, 4364.
- [26] C. Yang, F. P. Orfino, S. Holdcroft, *Macromolecules* **1996**, 29, 6510
- [27] H. Sirringhaus, P. J. Brown, R. H. Friend, M. M. Nielsen, K. Bechgaard, B. M. W. Langeveld-Voss, A. J. H. Spiering, R. A. J. Janssen, E. W. Meijer, P. Herwig, D. M. de Leeuw, *Nature* **1999**, 401, 685

- [28] R. J. Kline, M. D. McGehee, E. N. Kdnikova, J. Liu, J. M. J. Frechet, *Adv. Mater.* **2003**, 15, 1519.
- [29] M. S. A. Abdou, X. Lu, Z. W. Xie, F. Orfino, M. J. Deen, S. Holdcroft, *Chem. Mater.* **1995**, 7, 631
- [30] Zen, J. Pflaum, S. Hirschmann, W. Zhuang, F. Jaiser, U. Asawapirom, J. P. Rabe, U. Scherf and D. Neher, *Adv. Funct. Mater.* **2004**, 14, 757
- [31] Zen, D. Neher, K. Silmy, A. Holländer, U. Asawapirom and U. Scherf, *Jap. J. Appl. Phys.* **2005**, 44, 3721
- [32] H. Sirringhaus, N. Tessler and R. H. Friend: *Science* **1998**, 280, 1741
- [33] H. Sirringhaus, N. Tessler and R. H. Friend, *Synth. Met.* **1999**, 102, 857
- [34] J. A. Merlo and C. D. Frisbie, *J. Polym. Sci., Part B: Polym. Phys.* **2003**, 41, 2674
- [35] T. C. Gorjanc, I. Levesque and M. D'lorio, *Appl. Phys. Lett.* **2004**, 84, 930
- [36] S. K. Park, Y. H. Kim, J. I. Han, D. G. Moon, W. K. Kim and M. G. Kwak, *Synth. Met.* **2003**, 139, 377
- [37] G. Horowitz, R. Hajlaoui, R. Bourgouiga, M. Hajlaoui, *Synth. Met.* **1999**, 101, 401
- [38] A. R. Brown, C. P. Jarrett, D. M. Leeuw, M. Matters, *Synth. Met.* **1997**, 88, 37
- [39] G. Horowitz, *Adv. Mater.* **1998**, 10, 365
- [40] A. J. Heeger, S. Kivelson, J. R. Schrieffer, W.-P. Su, *Rev. Mod. Phys.* **1988**, 60, 781
- [41] P. J. Brown, H. Sirringhaus, M. Harrison, M. Shkunov, R. H. Friend, *Phys. Rev. B* **2001**, 63, 125204.
- [42] Y. H. Kim, D. Spiegel, S. Hotta, A. J. Heeger, *Phys. Rev. B* **1988**, 38, 5490.
- [43] F. Ebisawa, T. Kurokawa, and S. Nara, *J. Appl. Phys.* **1983**, 54, 3255.
- [44] J. H. Burroughes, C. A. Jones, and R. H. Friend, *Nature* **1988**, 335, 137.
- [45] C. Clarisse, M. T. Riou, M. Gauneau, and M. Le Contellec, *Electron. Lett.* **1988**, 24, 674.

- [46] A. Assadi, C. Svensson, M. Willander, and O. Inganäs, *Appl. Phys. Lett.* **1988**, 53, 195.
- [47] J. Paloheimo, E. Punkka, H. Stubb, and P. Kuivalainen, *Proceedings of NATO ASI* **1989**, Spetses, Greece, Plenum Press, New York.
- [48] G. Horowitz, D. Fichou, X. Z. Peng, Z. G. Xu and F. Garnier, *Solid State Commun.* **1989**, 72, 381.
- [49] G. Horowitz, X. Peng, D. Fichou, and F. Garnier, *Synth. Met.* **1992**, 51, 419.
- [50] F. Garnier, A. Yassar, R. Hajlaoui, G. Horowitz, F. Dellofre, B. Servet, S. Ries, and P. Alnot, *J. Amer. Chem. Soc.* **1993**, 115, 8716.
- [51] F. Garnier, R. Hajlaoui, A. Yassar, and P. Srivastava: “All polymer field-effect transistor realized by printing techniques” *Science* **1994**, 265, 1684.
- [52] A. Dodabalapur, L. Torsi, and H. E. Katz, *Science* **1995**, 268, 270.
- [53] C. D. Dimitrakopoulos, A. R. Brown, and A. Pomp, *J. Appl. Phys.* **1996**, 80, 2501.
- [54] R. C. Haddon, A. S. Perel, R. C. Morris, T. T. M. Palstra and A. F. Hebard, *Appl. Phys. Lett.* **1995**, 67, 121.
- [55] Z. Bao, A. Dodabalapur, A. J. Lovinger, *Appl. Phys. Lett.* **1996**, 69, 4108.
- [56] C. D. Dimitrakopoulos, B. K. Furman, T. Graham, S. Hegde, and S. Purushothaman, *Synth. Met.* **1998**, 92, 47.
- [57] Y.-Y. Lin, D. J. Gundlach, and T. N. Jackson, *54th Annual Device Research Conference Digest* **1996**, Santa Barbara, p. 80.
- [58] Y. -Y. Lin, D. J. Gundlach, S. F. Nelson and T. N. Jackson, *IEEE Electron Devices Lett.* **1997**, 18, 606.
- [59] H. Sirringhaus, R. H. Friend, X. C. Li, S. C. Moratti, A. B. Holmes, and N. Feeder, *Appl. Phys. Lett.* **1997**, 71, 3871.
- [60] H. E. Katz, A. J. Lovinger, and J. G. Laquindanum, *Chem. Mater.* **1998**, 10, 457.

- [61] J. G. Laquindanum, H. E. Katz, and A. J. Lovinger, *J. Amer. Chem. Soc.* **1998**, 120, 664.
- [62] H. E. Katz, A. J. Lovinger, J. Johnson, C. Kloc, T. Siergist, W. Li, Y.-Y. Lin, and A. Dodabalapur, *Nature* **2000**, 404, 478.
- [63] M. Halik, H. Klauk, U. Zschieschang, T. Kriem, G. Schmid, W. Radlik, and K. Wussow, *Appl. Phys. Lett.* **2002**, 81, 289.
- [64] P. R. L. Malenfant, C. D. Dimitrakopoulos, J. D. Gelorme, L. L. Kosbar and T. O. Graham, *Appl. Phys. Lett.* **2002**, 80, 2517.
- [65] C. Waldauf, P. Schilinsky, M. Perisutti, J. Hauch and C. J. Brabec, *Adv. Mater.* **2003**, 15, 2084.
- [66] S. Kobayashi, T. Takenobu, S. Mori, A. Fujiwara, and Y. Iwasa, *Appl. Phys. Lett.* **2003**, 82, 4581 (2003).
- [67] T. W. Kelly, L. D. Boardman, T. D. Dunbar, D. V. Muyres, M. J. Pellerite and T. P. Smith, *J. Phys. Chem. B.* **2003**, 107, 5877.
- [68] Th. B. Singh, N. Marjanović, G. J. Matt, S. Günes, N. S. Sariciftci, A. Montaigne Ramil, A. Andreev, H. Sitter, R. Schwödiauer and S. Bauer, *Mater. Res. Soc. Symp. Proc.* 2005, 871E, Warrendale, PA, I 4.9.1.
- [69] R. J. Chesterfield, C. R. Newman, T. M. Pappenfus, P. C. Ewbank, M. H. Haukaas, K. R. Mann, L. L. Miller, C. D. Frisbie, *Adv. Mater.* **2003**, 15, 1278.
- [70] B.H. Hadamani, D. Natelson, *Appl. Phys. Lett.* **2004**, 84, 443.
- [71] R. J. Chesterfield, J. C. McKeen, Ch. R. Newman, C. D. Frisbie, P. C. Ewbank, K. R. Mann and L. L. Miller, *J. Appl. Phys.* **2004**, 95, 6396.
- [72] C. Masayuki, S. Nagamatsu, T. Taima, Y. Yoshida N. Sakai, H. Yokokawa, K. Saito K. Yase, *Appl. Phys. Lett.* **2005**, 85, 2396.
- [73] G. Wang, T. Hirasa, D. Moses, A. J. Heeger, *Synth. Met.* **2004**, 146, 127.

- [74] T. D. Anthopoulos, C. Tanase, S. Setayesh, E. J. Meijer, J.C. Hummelen, P. W. M. Blom, and D. M. de Leeuw, *Adv. Mater.* **2004**, 16, 2174.
- [75] Th. B. Singh, N. Marjanović, G. J. Matt, S. Gunes, N. S. Sariciftci, A. Montaigne Ramil, A. Andreev, H. Sitter, R. Schwödiauer and S. Bauer, *Organic Electronics* **2005**, 6, 105.
- [76] Y. Wu, P. Liu, S. Gardner and B. S. Ong, *Chem. Mater.* **2005**, 17, 221.
- [77] L. A. Majewski, R. Schroeder, M. Voigt and M. Grell, *J. Phys.D: Appl. Phys.* **2004**, 37, 3367.
- [78] M. Chikamatsu, S. Nagamatsu, Y. Yoshida, K. Saito, K. Yase, and K. Kikuchi, *Appl. Phys. Lett.* **2005**, 87, 203504.
- [79] M. Heeney, C. Bailey, K. Genevicius, M. Shkunov, D. Sparrow, S. Tierney, and Iain McCulloch, *J. Am. Chem. Soc.* **2005**, 127, 1078.
- [80] E. Mizuno, M. Taniguchi, T. Kawai, *Appl. Phys. Lett.* **2005**, 86, 143513

List of Figures

| | | |
|-----------------|---|----|
| Figure 1 | Schematic structure of a bottom gate bottom contact OFET | 1 |
| Figure 2 | Possible device structures commonly used for organic field effect transistors. a) top contact / bottom gate, b) bottom contact / bottom gate, c) bottom contact / top gate, d) top contact / top gate [3]..... | 2 |
| Figure 3 | Energy level diagrams explaining the working principles of an OFET [3]..... | 3 |
| Figure 4 | Cross section of an OFET in three basic operation regimes: (a) for $V_d \ll V_g - V_{th}$ I_{ds} is linearly depending on V_d (linear regime), (b) At $V_d = V_g - V_{th}$ the conductive channel is pinched off, (c) for $V_d \gg V_g - V_{th}$ I_{ds} doesn't depend on V_d and has a constant value (saturation regime) [5]..... | 4 |
| Figure 5 | (a) Scheme of top contact PTV OFET. (b) Output characteristics (I_{ds} versus V_d) of a p-channel PTV OFET. (c) Transfer characteristics ($\sqrt{I_{ds}}$ versus V_g for different V_d). Linear field effect mobility of $7 \times 10^{-4} \text{ cm}^2 \text{Vs}^{-1}$ and saturated mobility of $10^{-3} \text{ cm}^2 \text{Vs}^{-1}$ can be extracted from these devices with channel length L of 25 μm and channel width W of 1.4 mm (W/L = 40). [3]..... | 5 |
| Figure 6 | Representative current-voltage curves of an n-channel organic field effect transistor. (a) Output characteristics indicating linear and saturation regime. (b) Transfer characteristics in the linear regime indicating the onset voltage (V_{on}) where the drain current increases abruptly. (c) Transfer characteristics in the saturation regime indicating the threshold voltage V_{th} where the linear fit to the square root of the drain current intersects with the x axis..... | 6 |
| | In this section the evolution of organic semiconductors for use in OFETs is presented with respect to their processing conditions and field-effect μ in Table 1. The chemical structures of most commonly used p-type and n-type semiconductors are presented in Figure 7 and 8..... | 9 |
| Table 1 | Highest field-effect mobility (μ) values measured from OTFTs as reported in the literature annually from 1986 through 2005. (taken from [3])..... | 9 |
| Figure 7 | Commonly used p-type organic semiconductor: F8T2 (poly[9,9' dioctyl-fluorene-co-bithiophene]); MDMO-PPV(poly[2-methoxy-5-(3,7-dimethyloctyloxy)]-1,4-phenylenevinylene); P3HT: regioregular poly [3-hexylthiophene]; PTAA: polytriarylamine; PVT: poly-[2,5-thienylene vinylene];, DH-5T: (α , ω -dihexylquinquethiophene); DH-6T: (α , ω -dihexylsexithiophene); phthalocyanine, pentacene, (α -6T) α -sexithiophene..... | 11 |

| | |
|---|----|
| Figure 8 Commonly used n-type organic semiconductor: NDI: naphthalene diimide; F ₁₆ CuPc :perfluorocopperphthalocyanine; Perylene; PTCDA: 3,4,9,10-perylene-tetracarboxylic dianhydrid and its derivaties; PDI: N, N'.dimethyl 3,4,9,10, perylene tetracarboxylicdiimide; C ₆₀ ; and PCBM : methanofullerene [6,6]-phenyl C ₆₁ -butyric acid methyl ester. | 12 |
| Figure 9 Schematic of a Michelson Interferometer | 13 |
| Figure 10 Data collection in FTIR spectroscopy. Two interferograms are recorded. Each of these is Fourier transformed to produce single beam spectra I ₀ and I respectively. Finally, I is divided by I ₀ to yield the (%T) transmittance spectrum.[12]..... | 16 |
| Figure 11 Evanescent wave penetrating in the device (MIS or transistor) built on ATR crystal | 17 |
| Figure 12 device structure of Bottom Gate / Top Contact organic transistor, used for the systematic study with different organic dielectrics | 19 |
| Figure 13 Chemical structure of organic semiconductors used for the device preparation, pentacene, phthalocyanine, P3HT (poly(3-hexylthiophene)) | 20 |
| Figure 14 Chemical structure of organic dielectrics used for the systematic study, PMMA (polymethyl methacrylate), PVP (polyvinyl phenol), CyEPL (cyanoethylpullulan), PVA (polyvinyl alcohol), BCB (divinyltetramethyldisiloxanebis(benzocyclobutene)), polyimide. | 21 |
| Table 2 Dielectric constants and capacitance per unit area of organic dielectrics used for device preparation | 21 |
| Figure 15 Device structure of transistors with P3HT as semiconductor and Au as source-drain electrodes on top of Si/SiO ₂ wafer (bottom contact / bottom gate). | 23 |
| Figure 16 Device structure of (BG/TC) transistors with P3HT as semiconductor on top of Si/SiO ₂ wafer (silicon acting as a gate electrode) with interdigitated Au source and drain electrodes (channel length L=25 μm)..... | 24 |
| Figure 17 The evolution of FTIR measurement: applied gate voltage and scanning versus time..... | 27 |
| Table 3 List of all materials used for the experiments | 29 |
| Table 4 Mobility values calculated for pentacene transistors with various organic dielectrics, using Au source- and drain-electrodes, L = 60 μm, W = 1.5 mm..... | 30 |
| Figure 18 Transfer characteristics of pentacene OFETs with different dielectrics (PMMA (polymethyl methacrylate), PVP (polyvinyl phenol), polyimide) and Au as source-drian electrodes. Ambipolar transport is evident in OFETs with PVP and PI gate dielectrics. Significant hysteresis is observed in these devices. | 31 |

| | |
|--|----|
| Figure 19. Transfer characteristics of pentacene OFETs with different dielectrics (CyEPL (Cyanoeethylpullulan), PVA (polyvinyl alcohol), BCB (divinyltetramethyldisiloxane bis(benzocyclobutene))). Ambipolar transport is observed in OFETs with PVA and CyEPL dielectrics. | 31 |
| Figure 20 Transfer characteristics of pentacene transistors with Ca/Al electrodes using various dielectrics (PMMA (polymethyl methacrylate), PVP (polyvinyl phenol), polyimide (PI), CyEPL (cyanoeethylpullulan)) | 32 |
| Table 5 Mobility values calculated for pentacene transistors with various organic dielectrics, using Ca/Al source- and drain-electrodes, L = 60 μm , W = 1.5 mm | 32 |
| Table 6 Mobility values calculated for zinc phthalocyanine transistors with various organic dielectrics using Au source- and drain-electrodes: | 33 |
| Figure 21 Comparison of transfer characteristics of a zinc phthalocyanine transistor with polyimide as dielectric measured under Argon atmosphere and in air. | 34 |
| Figure 22 Transfer characteristics measured in Ar atmosphere for phthalocyanine OFETs with different dielectrics (CyEPL (Cyanoeethylpullulan), PVA (polyvinyl alcohol), BCB (divinyltetramethyldisiloxane bis(benzocyclobutene)), PMMA (polymethyl methacrylate), PVP (polyvinyl phenol), PI (polyimide). Only the device using CyEPL shows ambipolar transport..... | 34 |
| Figure 23 Output characteristics of P3HT-OFETs scheme as shown in Figure 15 indicating hole-enhanced mode. Applied gate voltages are indicated for respective curves..... | 35 |
| Figure 24 Transfer characteristics of P3HT OFETs scheme as shown in Figure 15 for drain voltage of -40 V..... | 36 |
| Figure 25 Capacitance measurements of Si/SiO ₂ /P3HT/Au-MIS-Structure..... | 37 |
| Figure 26 Output characteristics of P3HT-transistor on Si/SiO ₂ with interdigitated electrodes, taken in the glovebox under N ₂ atmosphere | 38 |
| Figure 27 Output characteristics of P3HT-transistor on Si/SiO ₂ with interdigitated electrodes, taken in the FTIR-Spectrometer under N ₂ atmosphere after transport through air | 38 |
| Figure 28 Transfer characteristics of P3HT-transistor on Si/SiO ₂ with interdigitated electrodes, taken in the glovebox under N ₂ atmosphere | 39 |
| Figure 29 Transfer characteristics of P3HT-transistor on Si/SiO ₂ with interdigitated electrodes, taken in the FTIR-Spectrometer under N ₂ atmosphere after transport through air | 39 |
| Figure 30 Difference spectrum of MIS structure P3HT on Si/SiO ₂ | 41 |
| Figure 31 Absorption spectrum of chemically doped P3HT..... | 42 |

| | |
|--|----|
| Figure 32 Comparison of chemically doped P3HT with voltage induced absorption spectrum in the IR/V-bands region ($800\text{-}1600\text{ cm}^{-1}$) | 43 |
| Figure 33 Difference spectrum of P3HT-transistor on Si/SiO ₂ | 44 |
| Figure 34 (a) Schematic of a FET device in the bottom contact geometry for infrared characterization of charge injection. The active material in the FET devices is P3HT. (b) The <i>I-V</i> curve of a representative TiO ₂ -based FET (Figure taken from [11]) | 45 |
| Figure 35 The voltage-induced absorption spectra Δad for the P3HT layer under applied gate voltages V_{gs} in a TiO ₂ -based device. The green curve is a theoretical modelling of the experimental spectrum. (inset) Δad spectrum for a representative TiO ₂ -based device at $V_{gs} = -30\text{ V}$ along with the data for chemically doped P3HT [11]. The latter is the difference spectrum between the absorption of chemically doped P3HT with 1 mol % PF ₆ ⁻ and that of pure P3HT [11] scaled by a factor of 4×10^5 . (Figure taken from [11])..... | 45 |

Curriculum Vitae

Pinar Frank (née Senkarabacak)
Johann Wilhelm Kleinstrasse 72
A-4040 Linz
Telephone: +43 (0)699 81416554
E-mail: Pinar.Frank@jku.at

Personal Data

Date/Place of Birth: September 26th 1981 in Istanbul, Turkey
Nationality: Turkish

Education

01/2006 – 05/2007 Diploma Thesis at the Linz Institute for Organic Solarcells
10/2000 – 05/2007 Johannes Kepler Univeristy Linz
“Technische Physik”
09/2003 – 03/2004 Universidad de Granada, Spain
Exchange semester (Erasmus)
06/2000 School leaving exam at Sankt Georgs Kolleg Istanbul
(passed with distinction)

Language and Computer Skills

Languages Turkish (native)
German, English (fluent)
Spanish (elementary)
Computer MS Office, MS Origin, LaTeX, Mathematica
Basic knowledge of C and Fortran

Award

2000 – 2007 Scholarship of ALEV (Austrian College Foundation, Turkey)

Related Experience

10/2004 – 06/2005 Tutor for Grundlagen der Physik 1 and 2

02/2006 – 06/2006 Tutor for Thermodynamik and Statistische Physik

Tutor for Höhere Quantentheorie

04/2004 – 06/2004 Practicum at Linz Institute of Organic Solarcells
(Hybrid Solar Cells)

Interests / Private

Literature, Travelling, Science

Publication

“*Organic inverter circuits employing ambipolar pentacene field-effect transistors*”,
Th. B. Singh, P. Senkarabacak, N. S. Sariciftci, A. Tanda, C. Lackner, R. Hagelauer,
and Gilles Horowitz, *Appl. Phys. Lett.* 89, 033512 (2006),

Conference Attendance

2/2007 “*Probing of organic semiconductor – organic dielectric interface with FTIR/ATR method*” P. Senkarabacak, Th. B. Singh, H. Neugebauer and N. S. Sariciftci
Poster presentation at Winterschool on “Organic Electronics”,
Planneralm (Austria)